Applications and future developments of the (thermo-) poro-elastic theory in geophysics

Article *in* Earth-Science Reviews · November 2024

DOI: 10.1016/j.earscirev.2024.104996

7 authors, including:

Massimo Nespoli
University of Bologna
49 PUBLICATIONS **301** CITATIONS
SEE PROFILE

Hongyu Yu
Zhejiang University
32 PUBLICATIONS **434** CITATIONS
SEE PROFILE

Antonio Pio Rinaldi
ETH Zurich
167 PUBLICATIONS **3,964** CITATIONS
SEE PROFILE

Maria Elina Belardinelli
University of Bologna
103 PUBLICATIONS **1,454** CITATIONS
SEE PROFILE

Earth-Science Reviews 260 (2025) 104996

Contents lists available at ScienceDirect

Earth-Science Reviews

journal homepage: www.elsevier.com/locate/earscirev

Applications and future developments of the (thermo-) poro-elastic theory in geophysics

Massimo Nespoli [a,*], Hongyu Yu [b], Antonio Pio Rinaldi [c], Rebecca Harrington [d], Maria Elina Belardinelli [a], Giovanni Martinelli [e,f], Antonello Piombo [a]

[a] University of Bologna, Department of Physics and Astronomy "Augusto Righi", Viale Berti Pichat, 8, 40127 Bologna, Italy
[b] School of Earth Sciences, Zhejiang University, 866 Yuhangtang Road, 310058 Hangzhou, China
[c] Swiss Seismological Service, ETH Zurich, Sonneggstrasse 5, 8092 Zurich, Switzerland
[d] Institute for Geology, Mineralogy, and Geophysics, Ruhr University Bochum, Universitätsstr. 150, 44780 Bochum, Germany
[e] Dipartimento di Scienze Chimiche e Geologiche, Università degli Studi di Modena e Reggio Emilia, Modena, Italy
[f] Institute of Eco-Environment and Resources, Chinese Academy of Sciences (CAS), Lanzhou, China

ARTICLE INFO

Keywords
Thermo-Poro-elasticity
Fluids
Induced Seismicity
Faults
Reservoir
Geothermal systems
Inclusions

ABSTRACT

Fluids are naturally present in the crust from subsoil to several kilometers deep. The representation of the Earth's crust as a purely elastic medium ignores the effects of fluids within rock pores. Because the presence of fluids alters the mechanical response of rocks, the theory of poro-elasticity can be used to more accurately represent the deformation and the stress field of the crust, especially when the fluid saturation of rocks is high. In a poro-elastic medium, fluids interact with the hosting rocks through the pore-pressure. If the fluids have significantly different temperatures compared to the surrounding rocks, the theory of poro-elasticity can be generalized to the thermo-poro-elasticity, which also takes into account the effects of the thermal expansion of the medium The geophysical applications of these theoretical frameworks are highly diverse and based on different modeling approaches and assumptions. In this work, we emphasize potential applications of thermo-poro-elasticity theory in developing increasingly complex models of rock-fluid interactions. To do that, we focus on the different modeling approaches employed in some recent models of deep fluid exploitation, reservoir induced seismicity, interaction between seismic faults and fluids, and hydrothermal systems in volcanic zones. Our review paper aims to offer a comprehensive summary of the models, theories, code packages, and applications pertinent to this area and suggest some possible future developments of thermo-(poro-elastic) models in different application areas.

1. Introduction

Even if the presence of fluids in the subsoil has been known for a long time, the debate about their importance in characterizing and influencing geophysical phenomena is still open. The most abundant crustal fluids are water, CO_2 and hydrocarbons (mostly CH_4) (e.g. Fyfe, 1978). The subsoil water is mainly produced in the atmosphere and reaches the crust during the groundwater recharge. The water can accumulate and flow in the permeable soils that characterize the shallow crust giving rise to the *aquifers*, which may serve as an underground source of groundwater (Wang and Manga, 2021a). The latter can be recharged both by the direct infiltration of water from the surface and by water fluxes coming from the *recharge areas*, generally located in the mountains (e.g. Markovich et al., 2019). The water can be also transported down to the core-mantle boundary due to the lithospheric slabs at subduction zones (Karato et al., 2020; Walter, 2021). The CO_2 is mainly generated by metamorphic processes of crustal rocks and mantle degassing (e.g. Piombo et al., 2005). In particular, volcanic and hydrothermal areas are strong emitters of CO_2 (e.g. Chiodini et al., 2021). The magma near the Earth's surface, which is stored in crustal reservoirs, is a source of exsolved volatiles, primarily consisting of H_2O and CO_2 but also includes significant amounts of sulfur (H_2S and SO_2), carbon and halogen gasses (CO, HCl, HF), along with trace constituents such as volatile metals (Edmonds and Woods, 2018). The CH_4 in the Earth's crust is predominantly biogenic and derives from the degradation of organic matter from bacterial or thermogenic processes (Schoell, 1988).

Geophysical processes involving crustal fluids span a broad range of phenomena, such as ground subsidence, which is often due to

* Corresponding author.
E-mail address: massimo.nespoli2@unibo.it (M. Nespoli).

https://doi.org/10.1016/j.earscirev.2024.104996
Received 15 May 2024; Received in revised form 18 November 2024; Accepted 18 November 2024
Available online 23 November 2024

groundwater over-exploitation (Carminati and Martinelli, 2002; Holzer, 1984; Nespoli et al., 2021b; Teatini et al., 2006), induced seismicity in geo-energy related fluid injections/extractions (Ellsworth, 2013; Evans et al., 2012; Shapiro, 2015; Shapiro et al., 2010; Zang et al., 2014), stress and deformation induced in volcanological environments (Segall, 2010; Turcotte and Schubert, 2014) and the much debated topic of hydrological changes following earthquakes. The latter involve processes such as liquefaction, groundwater level changes, and post-seismic fluid flow, among others (Brodsky et al., 2003; Jónsson et al., 2003; Manga et al., 2012; Wang and Manga, 2010). Both theoretical and modeling approaches to represent such fluid related phenomena are characterized by high levels of complexity.

In this paper, we highlight the coupled interactions between Earth's crust and fluids within rock pore spaces, discussing the adequacy of pure elastic models in explaining geophysical observables during related transient processes. While we briefly address fluid-fault interactions, which is an important topic deserving of a dedicated study, the primary focus is on demonstrating the advantages of the poro-elastic framework for understanding fluid-rock matrix interactions. The following section will first introduce the distinct mechanisms in permeable, poro-elastic and thermo-poro-elastic media, providing a comprehensive review of the fundamental concepts, and governing equations, along with their respective responses under undrained/drained boundary conditions (Section 2). We further introduce representative porous-media applications in induced seismicity, geothermal and hydrocarbon exploitation, reservoir induced seismicity, fluid effects on fault reactivations and volcanic processes, covering geophysical observations, analytical approaches and evolution of numerical simulations (Sections 3 to 5). Section 6 highlights additional areas of poro-elasticity that are actively being explored in recent literature. Section 7 discusses emerging directions in various fields applying poro-elasticity theory, addressing current limitations due to the non-linear nature of the equations, and offering insights into unresolved challenges that call for the development of more advanced models. Overall, this structured exploration not only addresses the theoretical aspects but also underscores the practical significance of rock-fluid interactions, paving the way for future studies.

2. The dynamics of pore-fluids

2.1. Permeable media (P)

The simplest description of crustal fluid flow considers an incompressible single-phase fluid flowing in a porous and permeable medium. In this case, the *permeable medium* (P) is represented as a non-deformable solid matrix made up of small interconnected empty cavities (pores), within which fluid can flow (Fig. 1a). The solid matrix has a porosity (φ) which expresses the volume of pores per unit volume of the medium. If a cylindrical volume with section A and length L (Fig. 1a), is subjected to a vertical pore-pressure gradient

$$\nabla p = \frac{(p_2 - p_1)}{L} \tag{1}$$

a vertical fluid flow would occur. In this case, the ratio between the volume of fluids (Q, m^3/s) crossing a given section A of the medium in a second (Fig. 1a) expresses the magnitude of the Darcy's velocity (expressed in m/s):

$$q = Q/A \tag{2}$$

The empirical law describing the fluid flow occurring in a permeable media (Fig. 1a) is known as *Darcy's law* (Darcy, 1856):

$$\mathbf{q} = -\frac{k}{\eta}(\nabla p - \rho_f \mathbf{g}) \tag{3}$$

where $\mathbf{q}$ is the Darcy's velocity in its vector form, k (m^2) is the permeability of the medium, η (Pa s) is the fluid viscosity, ρ_f (kg/m^3) is the reference density of the fluid, and $\mathbf{g}$ (m/s^2) the gravitational acceleration. Permeability values in nature span over several orders of magnitude, from very permeable soils as gravel with $k = 10^{-7}$ m^2 to impermeable (or impervious) stones, such as granite, with $k = 10^{-20}$ m^2 (Bagdassarov, 2021; Turcotte and Schubert, 2014). Within this broad range, there are semi-permeable (or semi-pervious) materials. To model how the variation in fluid flow over time *t, Darcy's* law must be accompanied by the continuity equation (conservation of mass) which, by assuming the full saturation of the permeable medium in isothermal conditions, can be written as (Wang and Manga, 2021a):

$$\frac{\partial(\varphi\,\rho_f)}{\partial t} + \nabla\cdot(\rho_f \mathbf{q}) - \rho_f Q_s = 0 \tag{4}$$

where Q_s represents a generic source or a sink of fluid per unit volume of the medium (s^{-1}). Further complications to represent more realistic permeable media are then required to model the presence of: *i)* heterogeneity and anisotropy of the medium, *ii*) multiphase and multicomponent fluids, *iii*) heat and solute transport, *iv*) transient parameters describing the rock and the fluid phases. Such generalizations can be introduced analytically (Wang and Manga, 2021a; Ingebritsen et al., 2006) or by using very complex numerical codes such as HYDROTHERM (Kipp et al., 2008), TOUGH2 (Pruess et al., 2012), TOUGH3 (Jung et al., 2017) and COMSOL® (COMSOL, 2012), which are often used in both research and industry. In particular, the representation of multicomponent and multiphase fluids can be important when different components coexist in regions experiencing varying pressures and temperatures. Pressure and temperature regulate the phase (state of matter) of a material (solid, liquid, gas, or supercritical). The phase affects the material's physical properties, such as density and viscosity, which, in turn, influence the fluid dynamics within a porous medium. This is evident even in the basic principles of Darcy's law (Eq. (3)). Multicomponent and multiphase fluid representation becomes important for modeling

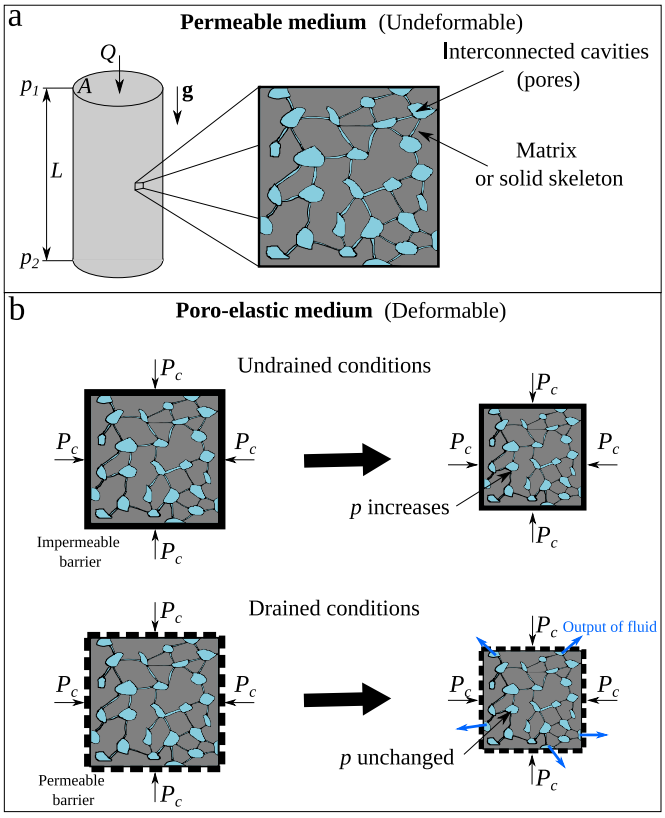

Fig. 1. Illustration of pore-fluids within a rock. Sketch of a (a) Permeable medium, (b) Poro-elastic medium.

systems in which different fluid phases and species share the same pore space. In such cases, the different relative permeability, capillary pressure and molecular diffusion of the fluids must be included in the models which become considerably more complicated. Examples of applications are CO_2 injection scenarios and hydrothermal systems, where CO_2 and H_2O can typically coexist in both liquid and gas phases (Borgia et al., 2017; Todesco et al., 2010).

2.2. Poro-elastic media (PE)

The description of a permeable medium neglects the mechanical effects of fluid-rock interaction (coupling). To describe a deformable, permeable medium, we can invoke the theory of poro-elasticity that was first derived by Biot (1941) and Terzaghi (1943) and subsequently extended by Geertsma (1966). Since surface deformation is one of the few direct observables in geophysics, poro-elastic theory is still commonly used in various applications, as we will see in the following.

A poro-elastic (PE) material is described by properties expressed per unit volume of the material. This *elemental volume* must be small enough to assume that all properties inside it are constant and change continuously between units, but large relative to the pore spaces or grain-size dimensions of the solid matrix. Media for which the above assumptions hold can be considered as a continuum. Within the theory of poro-elasticity, fluid diffusion can be represented by considering two different equations, according to Rice and Cleary (1976). The first is the constitutive equation linking strain e_{ij} and stress τ_{ij}. It is analogous to the constitutive equation of an elastic medium, except for the last term, which describes the pore-pressure change, p, within the continuum, with respect to a reference configuration and can be written as:

$$2\mu e_{ij} = \tau_{ij} - \frac{\nu}{1+\nu}\tau_{kk}\delta_{ij} + \frac{3(\nu_u - \nu)}{B(1+\nu)(1+\nu_u)}p\delta_{ij} \tag{5}$$

The term μ is the rigidity (Pa), δ_{ij} is the Kronecker delta function, B is the Skempton's coefficient (Skempton, 1954), ranging from 0 to 1, ν and ν_u are called *drained* and *undrained* Poisson's ratio, respectively, where $\nu \leq \nu_u \leq ½$. The Poisson's ratio terms are nondimensional. The second equation expresses the mass-balance and can be written as:

$$\Delta m = \frac{\rho_f}{\mu}\frac{3(\nu_u - \nu)}{2B(1+\nu)(1+\nu_u)}\left(\tau_{kk} + \frac{3}{B}p\right) \tag{6}$$

where Δm indicates the change in fluid mass content per unit of volume. To better understand the poro-elastic behavior we introduce two limiting conditions of the poro-elastic medium (e.g. Wang, 2000): the *undrained conditions* and the *drained conditions* (Fig. 1b).

2.2.1. The undrained conditions

The undrained conditions can be obtained by surrounding a sample of poro-elastic material with an impermeable jacket. In such a case, as the fluid is unable to flow out, an increase of the confining pressure P_c acting on the boundaries of the sample would lead to an increase of the pore-pressure p inside the pores, and vice-versa. The undrained conditions can be used to represent processes that occur on time scales which are too short to allow for the loss or gain of pore fluid in a material element, for which we can assume $\Delta m = 0$. In this case the relation between the pore-pressure and the stress is very simple:

$$p = -\frac{1}{3}B\tau_{kk} \tag{7}$$

with

$$B = \frac{3H(\nu_u - \nu)}{K(1+\nu_u)(1-2\nu)} \tag{8}$$

and

$$\frac{1}{H} = \frac{1}{K} - \frac{1}{K'_s} \tag{9}$$

where the Skempton's coefficient B is expressed in terms of the poro-elastic expansion coefficient, $1/H$ (Pa^{-1}), indicating the volumetric strain due to a change in p, K (Pa) the drained incompressibility of the poro-elastic medium and K'_s (Pa) which corresponds to the incompressibility of the solid portion of the medium, under some simplifying, but often assumed conditions (e.g. Wang, 2000). It is worth to notice that often in the literature the ratio

$$\alpha = \frac{K}{H} \tag{10}$$

is called Biot-Willis's coefficient.

2.2.2. The drained conditions

The drained conditions (Fig. 1b) represent the case in which a sample of poro-elastic material is surrounded by a permeable jacket. In this case an increase of the confining pore-pressure would be accompanied by a leakage of fluid from the sample which would tend to re-establish the pore pressure and for which we can assume that the pore-pressure change with respect to the initial state is $p = 0$ for a time $t \to \infty$. Therefore, for a sufficiently large time, the constitutive equation of a poro-elastic material (5) would be totally equivalent to the one of an elastic material. Actually, for the study of most of the transient phenomena in geophysics it is more interesting to study everything that happens between the conditions of undrained ($t \to 0^+$) and the condition of complete drainage ($t \to \infty$). Starting from the set of Eqs. (1) to (4), it can be shown that the dynamic of a poro-elastic medium which describes the transient mechanical effects can be expressed by the following system of equations:

$$\frac{\partial \tau_{ij}}{\partial x_j} = 0 \tag{11}$$

$$\nabla^2 e_{kk} - \frac{\partial^2}{\partial x_i \partial x_k}e_{ik} = 0 \tag{12}$$

$$\left(\frac{\partial}{\partial t} - D\nabla^2\right)\left(\tau_{kk} + \frac{3}{B}p\right) = 0 \tag{13}$$

where (11) are the equilibrium equations, (12) are the compatibility equations and (13) is the diffusion equation, D (m^2/s) is the hydraulic diffusivity (Rice and Cleary, 1976):

$$D = \frac{2k\mu B^2(1+\nu_u)^2(1-\nu)}{9\eta(1-\nu_u)(\nu_u - \nu)} \tag{14}$$

Notice that an additional term must be considered in Eq. (13) in cases in which fluid sources or sinks are present, as could be the case of models of fluid injection or withdrawal from wells. In absence of fluid sources or sinks, $Q_s = 0$.

2.3. A brief generalization to Thermo-Poro-Elastic media (TPE)

The generalization of the poro-elastic constitutive relation (5) to a thermo-poro-elastic (TPE) one (Selvadurai and Suvorov, 2016), which has the temperature change, T, as an additional variable, can be introduced following Biot (1941) and McTigue (1986):

$$2\mu e_{ij} = \tau_{ij} - \frac{\nu}{1+\nu}\tau_{kk}\delta_{ij} + \frac{3(\nu_u - \nu)}{B(1+\nu)(1+\nu_u)}p\delta_{ij} + \frac{2}{3}\mu\alpha_s T\delta_{ij} \tag{15}$$

where the last term of (15) depends on the coefficient of thermal expansion, α_s (K^{-1}), of the solid matrix. The diffusion Eq. (13) in absence of fluid sources or sinks can be also rewritten as (McTigue, 1986):

$$\left(\frac{\partial}{\partial t}-D\nabla^2\right)\left(\tau_{kk}+\frac{3}{B}p\right)=D\beta_1\nabla^2T+\beta_2\frac{\partial T}{\partial t} \tag{16}$$

with

$$\beta_1=\frac{4}{3}\mu\alpha_s\frac{(1+\upsilon)}{(1-\upsilon)} \tag{17}$$

and

$$\beta_2=\frac{2}{3}\mu B\varphi(\alpha_f-\alpha_s)(1+\upsilon)\frac{(1+\upsilon_u)}{(\upsilon_u-\upsilon)} \tag{18}$$

where $\alpha_f(K^{-1})$ is the thermal expansion of the fluid phase. The set of Eqs. (3), (4), (11) and (16) must be accompanied by the energy balance equation (Bejan, 2013):

$$\rho c\frac{\partial T}{\partial t}+\rho_f c_f\mathbf{q}\cdot\nabla T=\lambda\nabla^2T-\mathbf{q}\cdot\nabla p \tag{19}$$

where

$$\rho c=\left[\varphi\rho_f c_f+(1-\varphi)\rho_s c_s\right] \tag{20}$$

and

$$\lambda=\left[\varphi\lambda_f+(1-\varphi)\lambda_s\right] \tag{21}$$

with ρ_s the density of the solid matrix, c_s and c_f the specific heat (J kg^{-1} K^{-1}) of solid and fluid respectively, λ_s and λ_f the thermal conductivity (Jm^{-1} K^{-1}) of solid and fluid, respectively.

2.4. Effective stress and ΔCFS

In the literature is widely used the concept of *effective stress*, τ'_{ij}, which depends on pore pressure p and it can be expressed as $\tau'_{ij}=\tau_{ij}+\frac{K}{H}p\delta_{ij}$ (Kümpel, 1991; Wang and Manga, 2010), by assuming positive the tensile stresses. In materials with numerous and/or highly deformable cavities $K\ll K_s$, so $K/H\sim 1$ according to the Eq. (9). In this case the effective stress takes the simplified and often used form, $\tau'_{ij}=\tau_{ij}+p\delta_{ij}$. Its importance derives from the fact that strain is related to the effective stress in the same way as for an elastic medium: in other words, substituting τ_{ij} with τ'_{ij} the constitutive equation of a poro-elastic medium becomes formally identical to the one of a linear elastic medium. While most common computational approaches use the pore-pressure variation directly into a poro-elastic model and hence failure is evaluated with a given brittle or plastic criterion (e.g. Mohr-Coulomb, Drucker-Prager, Hoek-Brown, Cam-Clay, etc.), the stability of pre-existing fault planes due to local pore-pressure changes Δp can also be studied by computing the variations of the *Coulomb Failure Stress* (ΔCFS), which, neglecting the cohesion term variation, can be written as (e.g. Wang and Manga, 2010; Fan et al., 2019; Steacy et al., 2005):

$$\Delta CFS=(\Delta\tau)+f(\Delta\sigma_n+\Delta p) \tag{22}$$

where f is the static friction coefficient, on a given fault plane and $\Delta\tau$ and $\Delta\sigma_n$ indicate the changes in tangential and the normal stress (assumed negative for compressional loadings) acting on the same fault plane, respectively. According to Eq. (22) a positive pore pressure change can contribute to producing a positive Coulomb stress change. In this case, the slip on the fault plane, i.e. an earthquake, is favored. The criterion of Eq. (22) was largely and effectively applied in geophysical literature (Cocco and Rice, 2002; Jin, 2022; King et al., 1994; Nespoli et al., 2018; Nostro et al., 1997; Piombo et al., 2005). Generally, in undrained conditions, Δp can be computed from the volumetric stress change (the trace of the stress tensor), according to Eq. (7). Under the assumption that in a fault zone Δp is solely proportional to the normal stress acting on the fault plane ($\Delta p=-B\Delta\sigma_n$) the Eq. (22) can be rewritten, as often reported in literature, in terms of the effective friction coefficient, $f'=f(1-B)$ as (Beeler et al., 2000; Harris, 1998; Nostro et al., 2005):

$$\Delta CFS=(\Delta\tau)+f'(\Delta\sigma_n) \tag{23}$$

However, this assumption is not always verified. According to Cocco and Rice (2002), the Eq. (23) leads to the same results of the more general Eq. (22) only when:

- there is anisotropy near the fault plane, resulting in the strain component acting normal to the fault being much larger than those acting parallel to it,
- the rigidity of the medium near the fault is less than 50 % of that in the surrounding areas. This reduction could occur when porosity is dominated by cracks or flattened pores, with their long axes aligned subparallel to the fault plane.

Both conditions can be representative of a region surrounding a fault characterized by intensely fractured and compliant rocks (damage zone).

The limitations of *ΔCFS* analysis stem from the fact that it does not capture time-dependent processes, such as fault breakdown or healing, which are related to the evolution of fault properties. To model these processes, the pore-pressure changes must be incorporated into *rate- and state*-dependent friction laws, describing how the frictional strength of a fault evolves during sliding, due to the dependence on the slip rate (or velocity) and the evolving "state" of the fault surface subjected to a time-dependent effective normal stress (Dieterich and Linker, 1992). To model the coseismic evolution of a fault, several approaches that account for time-dependent pore pressure and porosity were proposed (Mitsui and Cocco, 2010; Segall and Rice, 1995).

3. Resource exploitation and induced seismicity

It has become widely recognized that poro-elasticity, in the broad sense, plays an essential role in the so-called induced seismicity: earthquakes generated by human activity. A recent review (Moein et al., 2023) summarized the physical mechanisms behind induced seismicity as stress perturbation:

- *Pore-pressure changes*: Fluids injected into or withdrawn from underground reservoirs alter the pressure in the pores of the rock and consequently the stress in the medium
- *Poro-elastic coupling*: Fluid injection or extraction causes the surrounding rock matrix to deform
- *Thermal stresses*: Injection of cold fluids or heat extraction result in thermal expansion or contraction of rocks which can induce stress
- *Earthquake interactions*: Once an earthquake occurs, it can influence the stress field of nearby faults, making them more susceptible to future earthquakes
- *Aseismic fault slip*: Sometimes, instead of causing a sudden seismic rupture, stress changes can induce slow, gradual movements along faults, known as aseismic slip that can redistribute stress in the medium.

Induced seismicity can be also related to fault weakening:

- *Stress corrosion*: This is a chemical process in which long-term exposure to stress and fluid interaction weakens the minerals in a fault zone
- *Dynamic weakening*: During seismic slip, frictional heating or rapid movement can lower the friction along the fault, allowing it to slip more easily
- *Cohesion loss*: Fault zones are held together by cohesive forces. If these cohesive forces weaken due to chemical, mechanical, or thermal processes, the fault becomes more susceptible to failure under stress.

In the following paragraphs, we summarized some of the fields (Fig. 2) where induced seismicity and poro-elasticity have been linked.

3.1. Geothermal

Geothermal exploitation is an important case study for poro-elasticity due to the presence of both permeable and fractured media. A geothermal system is a natural source of energy which can be extracted from the hot fluids permeating underground rocks. This operation is usually done with the extraction of the fluids through a well, however, in some cases, the permeability of the medium is insufficient to allow for the circulation of underground fluids, hence permeability must be artificially enhanced (*stimulation phase*). The first approach with direct production of hot fluid is commonly referred-to as "conventional" geothermal systems, while the second case is called as "unconventional" or "enhanced/engineered" geothermal systems (EGS) (Olasolo et al., 2016; Xie et al., 2015; Zimmermann and Reinicke, 2010).

For EGS, permeability enhancement can be achieved by injecting cold fluids, which causes the re-opening of the pre-existing fractures or the creation of new ones and a subsequent increase of the fluid flow in the host rocks (Fig. 2a). On the one hand, the challenge is to capture the greatest amount of heat from the Earth's crust, minimizing the work and costs. On the other hand, the geophysical literature is often focused on the study of the potential hazard and risks for the population that may be related to the production of energy from deep reservoirs and EGS. In fact, there are well-known cases in which underground energy exploitation was clearly linked to an increase of seismicity with respect to the natural seismicity observed prior to exploitation (Ellsworth, 2013; Evans et al., 2012; Ge and Saar, 2022; Grünthal, 2014; Keranen et al., 2014; National Research Council, 2013; Ritz et al., 2022; Shapiro et al., 2010; Silverii et al., 2021).

The importance of the seismicity induced by the exploitation of geo-resources has given rise to the creation of a decision support probabilistic tool such as the Adaptive Traffic Light System (ATLS) (Broccardo et al., 2019; Grigoli et al., 2017; Trutnevyte and Wiemer, 2017). As an example, the exploitation of the EGS of Basel (Switzerland) occurred in 2006 is a widely documented and studied case. There, the injection phase was planned to last 21 days, but it was initially reduced due to the high seismicity rate and then stopped after only 6 days due to the occurrence of a "large" M_L 2.6 earthquake. A subsequent M_L 3.4 earthquake occurred after shut-in at which point operators started the bleeding-off of the well. More than 10,000 earthquakes occurred during the whole stimulation around the injection well at about 4.5 km depth (Catalli et al., 2013; Häring et al., 2008; Rinaldi and Nespoli, 2017).

A very simplified approach by neglecting poro-elasticity is often already sufficient to explain the induced seismicity commonly observed in EGSs (e.g. Shapiro, 2015), especially during the stimulation phase, in which permeability enhancement is done. Some authors introduce the concept of seismogenic index which quantifies a seismogenic reaction of rocks to the impact of a fluid of unit volume: a higher seismogenic index implies a higher seismicity hazard related to fluid injections and a greater probability of earthquakes with great magnitude (Shapiro, 2018; Van Der Elst et al., 2016). A seismogenic index model, could in principle provide an easy relation between the induced seismicity and the injection flow volume during stimulation activity (Broccardo et al., 2019; Mignan et al., 2017), although not providing any substantial indication for permeability changes nor accounting for poro-elasticity. Such a method provides a straightforward approach to assessing seismic hazard by correlating seismicity with geological and geophysical parameters. But due to its empirical nature, the seismogenic index does not provide insights into the detailed physical processes that drive seismic events, and its predictions for the maximum magnitude of run-away ruptures could be unreliable. Very often the focus is more placed into the identification of the correct permeability enhancement rather than on stress changes due to poro-elastic coupling. For example, some modified versions of the TOUGH2/3 codes (Jung et al., 2017; Pruess et al., 2012) are widely used in scientific and industrial fields for their ability to represent multiphase and multicomponent fluids with a very high level of detail for both homogeneous (uniform poro-elastic behavior) and fractured (anisotropic poro-elastic behavior) media (Battistelli et al., 1997; Liu et al., 2020; Yuono and Daud, 2020; Zeng et al., 2013).

However, TOUGH2 does not consider the mechanical coupling between the fluid and the porous matrix, does not consider variations in permeability over time and by default would not allow to simulate seismicity. Recently, Rinaldi and Nespoli (2017) modified TOUGH2 to model the permeability changes that occur in a medium due to both elastic effects (as pressure increases, pores may expand, increasing permeability, or compress, reducing permeability) and permanent deformation caused by seismic events. In their model (TOUGH2-seed), they also integrated a seed-based method to simulate seismicity. The

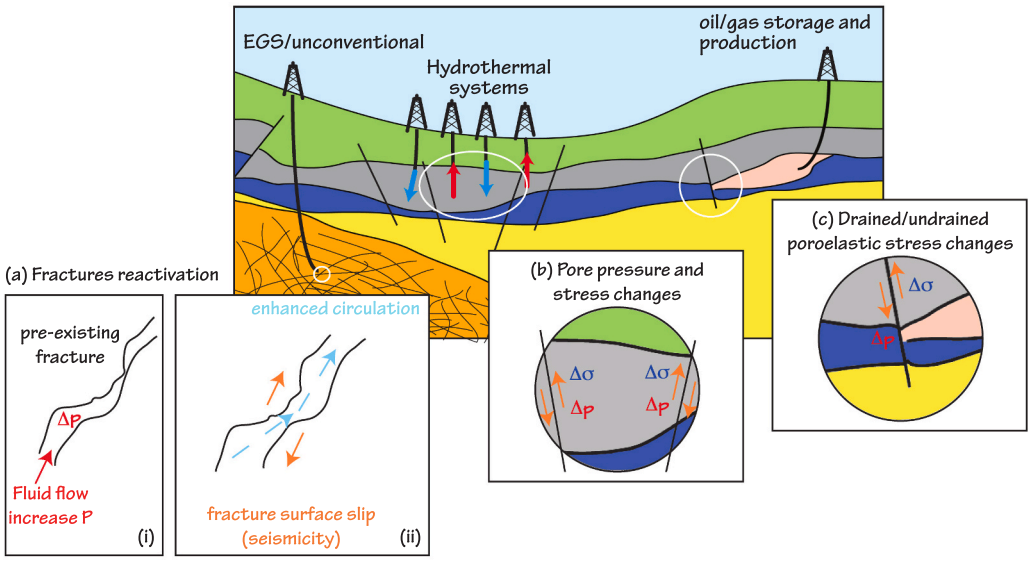

Fig. 2. Sketch of potential link between some common underground exploitation techniques and induced seismicity EGS system. (a) Pre-existing fracture reactivation during EGS, also referred to in literature as hydroshearing (e.g. Basel, Switzerland and Pohang, South Korea). (b) Pore pressure (Δp) and stress changes ($\Delta\sigma$) induced on faults (orange arrows indicate the slip direction) due to simultaneous production and re-injection of cold fluid in standard hydrothermal systems (e.g. Hengill, Iceland). (c) Poro-elastic undrained and drained response during gas production and injection (e.g. Groningen, Netherlands).

seed model (Gischig and Wiemer, 2013) consists of modeling possible earthquake location (seeds) within a domain, following an assigned spatial distribution. These seeds can trigger an earthquake depending on the changes in stress and pore pressure computed at their location. Despite the absence of poro-elasticity, the modeling approach was successfully applied to reproduce the case of induced seismicity by EGS at Basel (Rinaldi and Nespoli, 2017), seismicity linked to fluid-reinjection in conventional geothermal field of Hengill in Iceland (Ritz et al., 2020), as well as seismicity linked to geothermal investigations at *St.* Gallen (Zbinden et al., 2020a). TOUGH2-seed capabilities are very useful, however it should be considered that integrating permeability changes with seismicity predictions can be complex and may require extensive calibration and validation. Moreover, the accuracy of predictions of the TOUGH2-seed depends on the quality of input parameters and the assumptions made in the model.

The full coupling between fluid and the solid matrix, provided by the formalism of poro-elasticity (Section 2.2), is especially required when one is interested in modeling stress, deformation, and displacement fields associated with the injection/extraction of fluids. One possible method to analytically address the problem consists of representing the geothermal reservoir as an inclusion, following the method described by Eshelby (1957). According to this method, the reservoir is meant as a volume undergoing pore-pressure (and/or temperature) changes that is enclosed by an elastic medium. The literature following this approach focuses on studying the potential of a reservoir to induce seismicity (e.g. Geertsma, 1973; Rudnicki, 1999; Segall, 1992) and the associated displacement (e.g. Guido et al., 2015). In particular, inclusion models allow us to explain the different fault mechanisms (normal, reverse, and strike-slip faults) induced by geothermal activity within and outside the reservoir as was observed in some areas of the world (Segall, 1989; Segall and Fitzgerald, 1998). The solutions obtained through the Eshelby (1957) method are static, i.e., they allow calculation of the mechanical effects for assigned pore pressure (and/or temperature) changes and assume idealized conditions that may not fully represent real-world complexities, such as heterogeneous materials. A somewhat similar approach combines changes in stress and pore pressure with a rate-and-state model of seismicity to understand how induced seismicity evolves over time (Segall and Lu, 2015). They demonstrated that in areas where the background shear stress is relatively low (meaning that the faults are not critically stressed for failure), the seismicity rate is more strongly controlled by changes in pore pressure and stress caused by fluid injection or extraction. Furthermore, they found that poro-elastic effects can explain why larger seismic events may not occur immediately after injection begins but can become more likely as the system equilibrates during the shut-in phase.

An effective approach to model the transient nature associated with poro-elastic behavior due to injection and withdrawal of fluids in a multi-layered half-space, divided into multiple distinct layers, each with its own physical properties, is given by the POEL code (Wang and Kümpel, 2003). The solutions of POEL are based on the technique of the mirror-image and use Haskell's propagator method to represent the layering of the medium. Compared to the numerical codes that we have previously presented, POEL is suitable to represent single-phase and single-component fluids (e.g. water substance) and does not consider thermal effects on the fluid dynamics, but it accounts for the full mechanical coupling between the fluid and the solid matrix. Several recent works used the POEL code to model the mechanical effects that lead to induced seismicity (e.g. Deng et al., 2020; Silverii et al., 2021; Yu et al., 2019).

More complex THM (Thermo Hydro Mechanical) models are based on the fully coupled approach. For example, the TOUGH-FLAC code (Jeanne et al., 2015; Rinaldi et al., 2015; Rinaldi and Rutqvist, 2019; Zbinden et al., 2020b) is based on the coupling of TOUGH2/3 with the geomechanical software FLAC3D (Itasca, 2009). Other approaches of fully thermo-hydro-mechanical processes in EGS and induced seismicity include VISAGE (Koutsabeloulis and Hope, 1998), STARS (CMG, 2003), COMSOL® (e.g. Andrés et al., 2019; Cao et al., 2022; Chang et al., 2020) and CODE-BRIGHT (Alcolea et al., 2024; Boyet et al., 2023).

3.2. Oil/Gas injection and production

For these cases of geotechnical activities, poro-elasticity plays an essential role in understanding the cause of induced seismicity. In fact, the injection/production often occurs in permeable, soft reservoirs that are prone to large deformation. The deformation of the reservoir (compaction for production or general uplift for injection) is responsible for stress changes that consequently can lead to reactivation of faults when combined to pressure changes due to the injection or removal of fluids. In analogy with what occurs for geothermal energy, even the extraction of deep fluids, such as methane (widely used for the production of electricity), is followed by the re-injection of water or CO_2 (e.g. Karegar et al., 2015), to increase natural gas recovery and reduce CO_2 emissions in the atmosphere (Khan et al., 2013; Zhang et al., 2023).

In case of injection, such as the case of CO_2 storage, several models have been proposed to address the issue of induced seismicity (Cheng et al., 2023; Vilarrasa et al., 2019). TOUGH-FLAC, for example, gives the flexibility to use several equations of states and it was largely used to address both deformation linked to injection operation (Rinaldi et al., 2017; Rinaldi and Rutqvist, 2013; Rutqvist et al., 2002) as well as the potential for fault reactivation (Rinaldi et al., 2014; Rutqvist et al., 2016; Vilarrasa et al., 2017). Other commonly used codes for the topic of induced seismicity during carbon dioxide storage are CODE_BRIGHT (Vilarrasa et al., 2015, 2019), ECLIPSE-FLAC (Cao et al., 2021), CGM-STARS (Verdon et al., 2015), or TOUGH-PyLith (Blanco-Martín et al., 2022).

Both oil and gas extraction cause rock contraction due to the pore-pressure reduction in the reservoir. The change of pore-pressure can in turn lead to a change of the mass distribution inside the reservoir and then change the local stress field (e.g. Hough et al., 2017; Segall, 1989). For the case of production, one prominent example is certainly the case of gas production at the Groningen field in the Netherlands, where gas was extracted for more than 30 years before any seismicity occurred (Van Thienen-Visser and Breunese, 2015). There, the poro-elastic response closely aligns with observed data, as seismic activity tends to correspond with periods of high gas extraction and often shows a delayed response. This delay reflects the slow compaction of the reservoir and the gradual build-up of stress due to pressure drop in the reservoir. The observed increase in seismic events is consistent with the poro-elastic transfer of stress, while other mechanisms, such as pore fluid diffusion or thermoelastic effects, cannot fully account for the spatial and temporal patterns of seismicity observed at the Groningen field. Poro-elasticity (both drained and undrained effects) due to reservoir compaction is the only viable physical mechanism that nicely explains the occurrence of seismicity. For example, by using TOUGH-FLAC with a generic theoretical model, Zbinden et al. (2017) show that the compaction caused by the gas production leads to shear stress changes on a fault zone bounding the reservoir. They further show that re-injection in the same reservoir with the aim of restoring the initial pore pressure is only a partially effective countermeasure because it may not fully reverse the stress and compaction effects induced by extraction, and it could introduce additional complexities related to fluid flow and uneven pressure redistribution. By using semi-analytical Green function calculation, a more recent work by Smith et al. (2022) showed how correctly accounting for the stress variation in the case of Groningen could be useful to forecast the induced seismicity.

Often the gas/oil extraction is accompanied by subsequent reinjection of fluids. The challenge in this type of application is to identify the most effective re-injection strategies to ensure the stability and sustainability of the reservoir. Even if the production phase can induce earthquakes in the reservoir, in many cases induced seismicity has been observed during the re-injection phase (Cesca et al., 2021; Deng et al., 2020). From a geophysical point of view, the oil and gas production

models are similar to those commonly used in geothermal energy and allow us to simulate the injection and withdrawal of fluids at a given pore pressure and possibly a given temperature. For example, Deng et al. (2020) used the MODFLOW-2005 software (Harbaugh, 2005) to model the pore-pressure evolution due to fluid injection and oil and gas extraction in western Texas. They found that fluid injection is likely the main contributor to the observed induced seismicity as it increases pore pressure, reactivates faults, and shows strong temporal and spatial correlations with the observed seismic events.

There are also alternatives in the literature to model the coexistence of different chemical species within the study area (see for example Kutsienyo et al., 2021 and refs therein), such as TOUGHREACT (Xu et al., 2008), STOMP-EOR (White and Oostrom, 2006), and GEM simulators (CMG, 2021). In fact, in addition to the multiphase and multicomponent fluids representation, it may indeed be important to introduce geochemistry into the existing framework of thermo-poro-elasticity, leading to THMC (Thermo-Hydro-Mechanical-Chemical) models. In these cases, we talk about multiphase multicomponent reactive transport, where different chemical species interact with different phases in complex ways (Oliveira et al., 2018) as chemical reactions can occur between the different fluid phases. Chemical species can be transformed, potentially causing the precipitation or dissolution of solid minerals. These changes can alter the geometry of the pore space, which in turn affects the flow velocity field and transport processes like advection and diffusion (Mehmani and Balhoff, 2015). Moreover, also endothermic and exothermic reactions can influence the thermal budget of the system (Tao et al., 2019). Chemical reactions in THMC can occur on time scales that range from seconds to millions of years, depending on the type of reaction and environmental conditions. When modeling such systems, it is crucial to distinguish between reactions that occur rapidly and those that are significantly slower, as the latter may be negligible within the relevant time frame of the model.

3.3. Deformation and seismicity induced by dam-reservoirs

The theory of poro-elasticity finds application in another scenario which is still the subject of an interesting scientific debate today: the dam-reservoir (lake) induced seismicity. In the literature there are several works reporting evidence of seismicity induced by shallow hydrological loads in the Earth's crust. A review of studies on this topic was performed by Gupta (2002), according to which the largest induced earthquake had a M 6.3 and took place in India in 1967 at the Konya reservoir. For the purpose of this work, we aim at introducing the role of fluids and the theory of poro-elasticity in the interpretation and modeling of this phenomenon. The physical mechanisms at the base of the reservoir induced seismicity can act together and can be grouped in three different categories (Fig. 3):

i) *elastic response due to the variable loading of a reservoir level*. This arises from the fact that a column of water, with density ρ_w, exerts a pressure, p_s, at the bottom of the lake that depends on the water level h_w, so that $p_s = \rho_w g h_w$. An instantaneous vertical load at the top of the crust, represented as an elastic half-space, can be easily modeled by using the Boussinesq (1885) solutions and it may favor (or prevent) the generation of earthquakes around the reservoir. This occurs because hydrological loads alter the distribution of stress within the crust, especially near the surface and can induce seismicity, especially in regions where faults are near a critical stress state. Such solutions were used for example to model the mechanical state of the Atatürk Reservoir (Turkey) whose water impoundment was accompanied by two earthquakes with M > 5 in 2017 and 2018 (Büyükakpınar et al., 2021).
ii) *undrained poro-elastic response of fluids*. If, as is likely to be the case, the rocks surrounding the reservoir are water saturated, according to Eq. (7) the instantaneous deformation due to a change in water level is accompanied by a pore-pressure variation that can promote further seismicity with respect to the pure elastic response, according to the Eq. (22). Such an approach was employed for example to study the possible trigger effect on local faults due to the water level changes of the Pirrís Reservoir (central Costa Rica)(Ruiz-Barajas et al., 2019).
iii) *transient response of the fluid*. The importance of this third mechanism lies in the fact that it can justify induced seismicity that is delayed with respect to reservoir level variations. In fact, after the undrained response, the fluid permeating the rocks near the reservoir is in non-equilibrium conditions, and it must flow to reach a new equilibrium configuration, in a similar way to what happens after an earthquake, which will be dealt with in the next section. Furthermore, the sudden change of the load at the bottom of the reservoir can generate a pore pressure pulse that propagates downward from the reservoir into deeper depths.

To model the vertical diffusion at a depth, z, of the pore-pressure induced by a step load placed at the top of an half-space ($z = 0$),

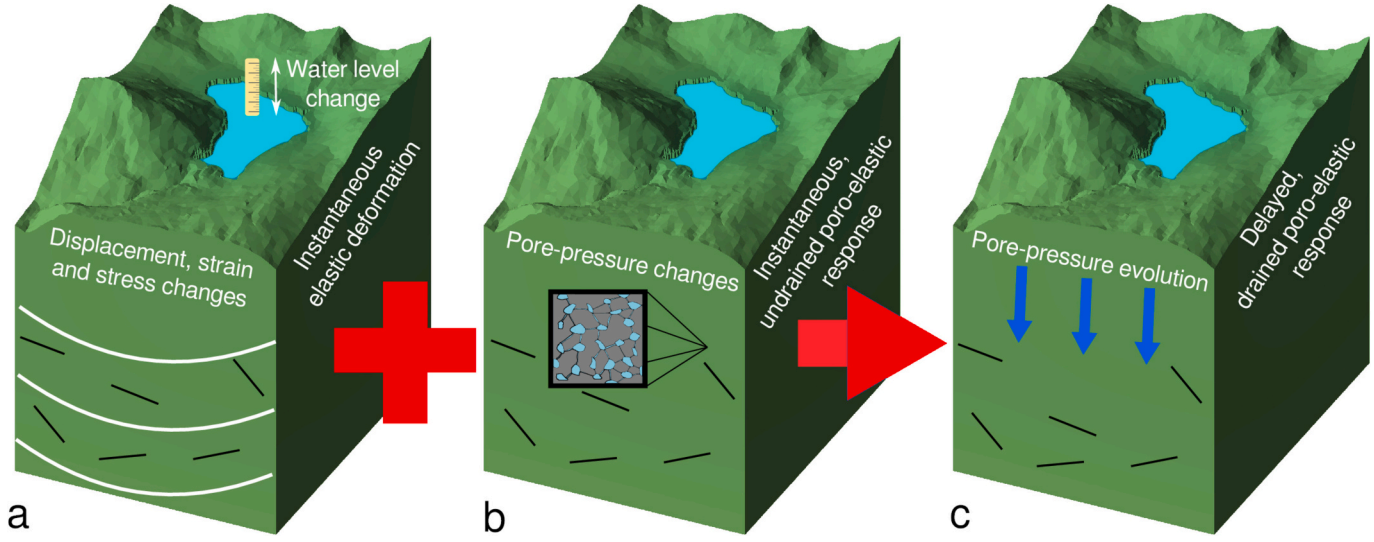

Fig. 3. Sketch of the effects of water level changes in a reservoir. (a) Instantaneous elastic response. (b) Instantaneous undrained poro-elastic response. (c) Evolving pore-pressure. Black segments represent pre-existing fractures and potential earthquake locations which can be induced by the three coupled mechanisms.

several authors assume the following analytical solution (Belferman and Agnon, 2024; Roeloffs, 1988; Wang, 2000):

$$p(z,t) = \gamma p_s + (1-\gamma)p_s erfc\left(\frac{z}{\sqrt{4Dt}}\right) \quad (24)$$

with

$$\gamma = B\frac{(1+\nu_u)}{3(1-\nu_u)} \quad (25)$$

where p_s is here assumed to be the pore pressure on the top of the half-space, γ is the loading efficiency (it can vary from 0 to 1) and *erfc* is the complementary error function. Notice that for $\gamma = 1$ the equation corresponds to assuming an instantaneous and uniform increase of the pore-pressure below the lake, i.e. $p(z, t) = p_s$. This last assumption was employed by Brothers et al. (2011) to show that the periodic flooding of the palaeo-Salton Sea had the potential to trigger earthquakes on the southern San Andreas fault. Starting from Eq. (24) was estimated that pore-pressure diffusion from the Itoiz Reservoir (Spain) can explain the observed M ≥ 3 earthquakes (Durá-Gómez and Talwani, 2010). Ge et al. (2009) suggested that the mechanical effects due to the presence of the Zipingpu Reservoir potentially accelerated the occurrence of the Wenchuan earthquake (China) by tens to hundreds of years.

More complex models enable a more realistic description of rock heterogeneity and the consequent three-dimensional diffusion patterns of fluids (e.g. Hill et al., 2023). Rinaldi et al. (2020) developed a method to study the seismicity associated with the impoundment and level changes of the Pertusillo Lake (Italy). Their methodology combines a semi-analytical poro-elastic model with an earthquake nucleation approach based on rate-and-state frictional law. By incorporating rate-and-state frictional law, the methodology can simulate how variations in stress and pore pressure influence fault behavior and the potential for earthquake nucleation. Furthermore, by studying the Longtan reservoir (China), Hua et al. (2013) suggest that the presence of permeable faults close to the lake can explain the presence of earthquakes that do not occur in its surroundings: in that case faults can act as preferential ways for pore-pressure diffusion and they extend the influence of the lake to greater spatial scales.

4. Seismic faults and fluids

It is widely known and accepted that earthquakes can affect groundwater leading to different hydrological responses (e.g. Manga and Wang, 2015). It is not equally clear when and how much the poro-elasticity can help to explain the earthquake effects that are usually observed at the surface. Fault zones are made up of a *fault core* surrounded by a *damage zone*. The fault core hosts most of the displacement due to the fault movement and it is characterized by high strains forming structures like breccias (fragments of broken rock) and gouge (fine-grained, clay-rich material) (Caine et al., 1996; Johri et al., 2014). The damage zone (Kim et al., 2004) is constituted by a network of smaller fractures and minor faults distributed around the fault core and it can be represented by a compliant rock volume (Segall, 2010). Beyond the damage zone there are the less compliant *host rocks*. The three structures can have different hydraulic characteristics and the ability of a fault zone to serve as a conduit or a barrier, is influenced by the relative proportions of fault core and damage zone structures (Caine et al., 1996): in fault zones with extensive damage zones, fluid flow is enhanced through a thin tabular region parallel to the fault plane, while the fault core limits fluid movement across the fault (Evans et al., 1997). In presence of a low-permeability gouge, which prevents the fast escape of fluids, *thermal pressurization* may occur (Wibberley, 2014). In such a case, the frictional heating generated during an earthquake along the fault plane can cause a rapid increase of the pore-pressure, significantly weakening the fault. In many study cases, a detailed description of the fault zone is lacking, making it difficult to attribute precise mechanical parameters to its heterogeneous structure. Consequently, faults are often modeled as surfaces with varying degrees of geometric complexity. This approximation allows us to easily use the dislocation theory to represent seismic faults.

4.1. Static and dynamic effects of fluids on faults

Generally, fluid-related earthquake phenomena can be distinguished as *static* and *dynamic* effects (Manga and Wang, 2015; Wang and Manga, 2014). While static effects may be dominant primarily in the near field (distance from the epicenter of about one fault length), dynamic effects are the only mechanisms that can lead to hydrological responses in the far-field (Manga and Wang, 2015). The static effects are related to permanent changes on the deformation field induced by an earthquake in the surrounding region, which can be modeled, as a first approximation, considering static dislocations located within an elastic half - space (e.g. Okada 1992 or Segall 2010). Static stress changes induced by an earthquake can lead to a reduction of the compressive normal stress acting on neighboring fault planes (receiving faults). The phenomenon, known as *fault unclamping* (Scholz, 2002) is critical because it entails a reduction of the frictional resistance or an increase of the Coulomb Failure Stress (Eq. (22)) on receiving faults. This condition can facilitate fault slippage, potentially leading to earthquake nucleation (King et al., 1994) or influencing the propagation of an existing rupture (Harris and Day, 1999). In undrained condition, i.e. during the coseismic stage, the pore pressure increase caused by static stress changes can lead to unclamping of faults as well, by reducing the compressive effective normal stress acting on a receiving fault (according to Eq. (22)), as we show in the next section. However, this pore pressure increase can be counteracted by dilatant effects, since fault slip may open additional fractures and lower the pore pressure.

The dynamics effects entail short-term and transient strain (and stress) variations due to the passage of seismic waves. Dynamic stress changes can either accelerate the time-to-failure of a fault or delay it (Belardinelli et al., 2003), even if their effectiveness tends to be more pronounced for critically loaded faults. Furthermore, seismic waves can lead to dynamic changes in pore pressure which can cause a fault to slip sooner than predicted by the static models (Brodsky and Kanamori, 2001). Even if such dynamic effects lead to temporary poro-elastic responses, they can be sufficiently strong to cause permanent permeability and porosity changes that vary the characteristics of the medium (Elkhoury et al., 2006; Manga et al., 2012; Wang and Manga, 2014). Among dynamic effects, we mention changes in water level, stream discharge rate, and water temperature (Brodsky et al., 2003; Kümpel, 1992; Roeloffs, 1998; Wang and Chia, 2008) as well as soil liquefaction (e.g. Minarelli et al., 2022; Subedi and Acharya, 2022). The undergoing physical mechanism is related to the energy carried by seismic waves that can break or move the obstacles to pore-fluid flow.

4.2. Coseismic poro-elastic effects

If the rocks are porous and host fluids, the deformation field induced by an earthquake must account for the stress coupling between the solid and the fluid provided by the theory of poro-elasticity which can be used (e.g. Roeloffs, 1996) to model both the co-seismic and post-seismic phases. In the co-seismic phase, since the rocks deform very quickly and the fluid contained in a deformed volume element has not yet had time to flow, the undrained conditions (Section 2.2.1) are valid (e.g. Wang, 2000). During the co-seismic phase, a pore pressure increase ($p > 0$) is expected in zones subjected to compression, while a decrease ($p < 0$) is expected in zones subjected to dilation (Fig. 4). The fluid flows that occur (Section 2.2.2) during the subsequent post-seismic phase arise to re-establish the equilibrium condition in terms of pore-pressure ($\mathbf{q} = 0$ in Eq. (3)). Deng et al. (2016) demonstrate the competing effects of the poro-elastic stress and pore pressure changes in their observations showing the triggering of earthquakes on short time scales after

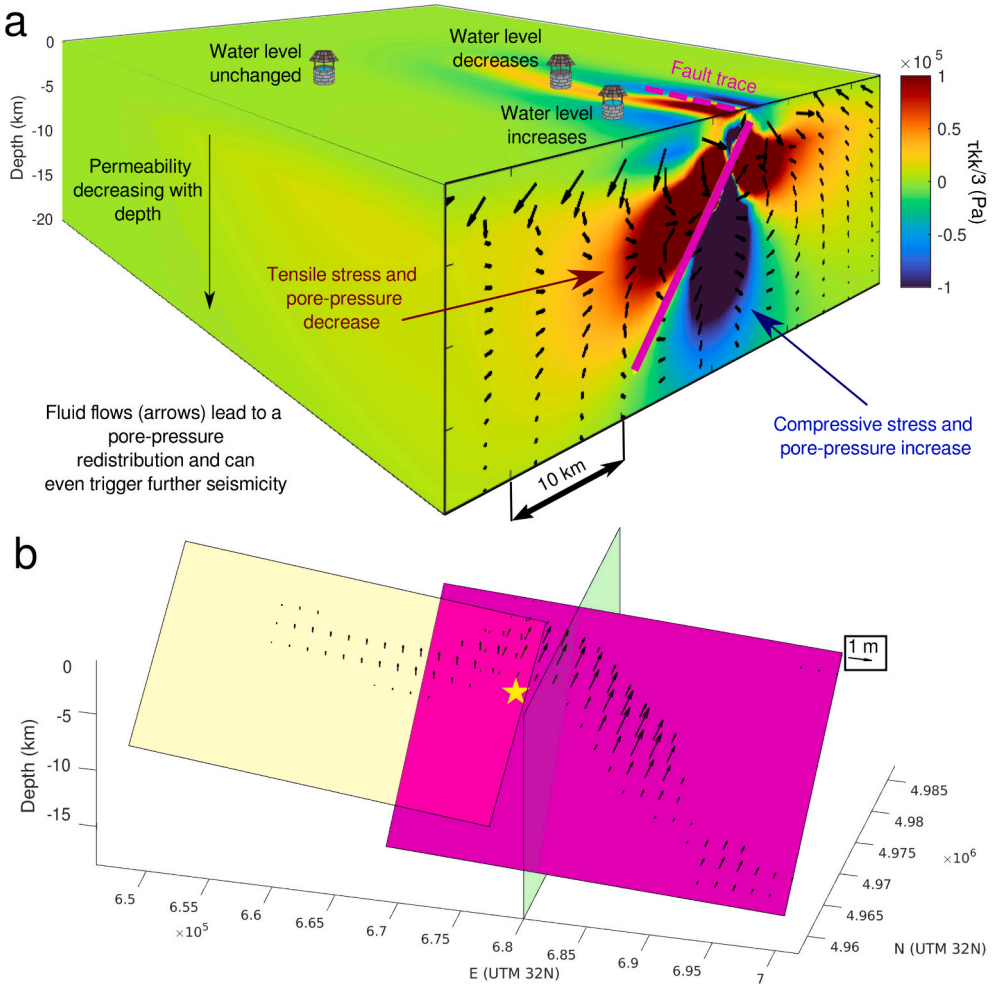

Fig. 4. 3D illustration of the coseismic isotropic stress component $\tau_{kk}/3$ (color) generated by the mainshock (Mw 6.1) of the 2012 Emilia-Romagna seismic sequence (Italy). (a) The fault plane hosting the mainshock is represented in the N-S vertical section with a pink line. At the surface the fault trace is also reported with a pink dashed line. The fault is a transpressive fault (rake angle = 70°) with a non-uniform slip distribution (see Nespoli et al., 2017, 2018 for further details). Darcy's velocities in logarithmic scale (black arrow on the vertical section) indicates the direction of the fluid flow which diverges from the compressed areas and converges in the dilated area. Velocities are computed assuming a permeability decreasing with depth. Expected water well responses according to the poro-elastic theory are also reported in the illustration. (b) Geometries of the two seismic faults (yellow and pink rectangles) with their slip distribution (black arrows). The hypocenter location of the mainshock is represented with a yellow star. The green rectangle shows the location of the N-S vertical section plotted in panel a. (For interpretation of the references to color in this figure legend, the reader is referred to the web version of this article.)

injection into low-permeability shales. The injection activity triggered earthquakes shortly after injection at distances over which pore pressure diffusion effects would be negligible. In contrast, the poro-elastic stress changes at the site of the induced earthquakes were estimated to be comparable to the magnitudes of stresses that have been observed to trigger earthquakes elsewhere.

It is worth noting that to compute the total poro-elastic rebound (after the complete drainage of the fluid) induced by a fault, one can simply compute the difference between the two coseismic, static responses, computed using the undrained υ_u and the drained, υ Poisson's moduli, respectively (Peltzer et al., 1998).

The poro-elastic response to an earthquake can be envisaged by observing the variations of the flow rate of the spring and the level of water wells (or piezometers), which are closely related to the pore pressure changes that occur at depth. In fact, a sudden increase of the water level

$$\Delta h = \frac{\Delta p}{\rho_f g} \tag{26}$$

is expected in response to increases of the pore-pressure while a sudden decrease is expected in zones undergoing a pore-pressure decrease (Ge and Stover, 2000; Jónsson et al., 2003; Nespoli et al., 2016). The correlation between the volumetric strain induced by earthquakes and water level changes was found as examples by Akita and Matsumoto (2004) for the M8.0 Tokachi-Oki (Japan) earthquake of 2003, Nespoli et al. (2016) for the M6.1 Emilia-Romagna earthquake (Italy) of 2012, Lai et al. (2021) for the M7.9 Wenchuan Earthquake (China) of 2008. Other interesting cases are reported by Wang and Manga (2021b) and references therein.

4.3. Postseismic poro-elastic effects

An example of the expected poro-elastic response due to a strike-slip fault is shown in Fig. 5. The evolution of the pore-pressure computed in the two locations P1 and P2 is consistent with the poro-elastic responses that can be observed in water wells: a sudden change followed by a slow recovery due to the fluid flow.

However, there are also several cases in which only the static deformation due to an earthquake is not sufficient to explain the coseismic water level changes and their subsequent evolution. Other physical mechanisms have been proposed for these cases, including

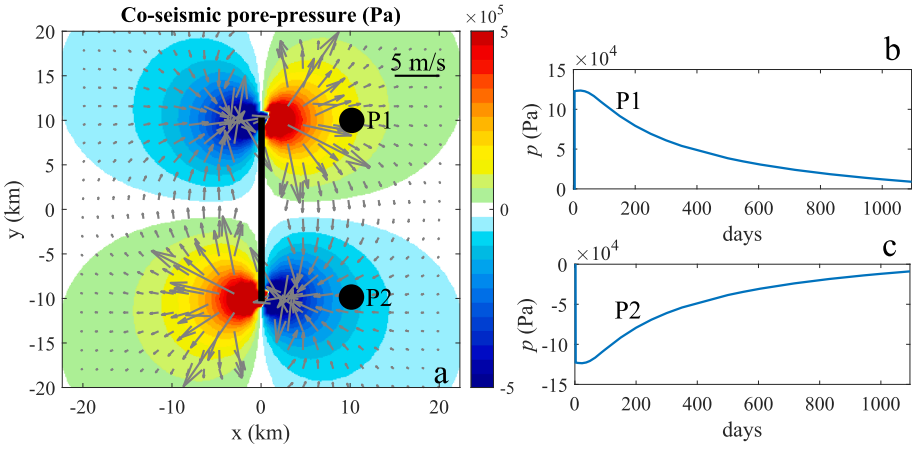

Fig. 5. Poro-elastic response of a left lateral strike slip fault. (a) Map of co-seismic pore-pressure. The gray arrows indicate the Darcy velocities (**q**). The black line is the fault trace. The two circles indicate the location of two query points P1 and P2 whose pore-pressure evolution is shown in panels (b) and (c), respectively. The top of the faults is 1 km, the length is 20 km and the width is 10 km. The strike is 0°N. The dip is 90°. The poro-elastic parameters are pertinent to describe the Ruhr sandstone (Wang, 2000): μ =13 GPa, $\upsilon = 0.12$, $B = 0.88$, $D = 5.3{\cdot}10^{-3}$ m^2/s, $\alpha = 0.65$. The magnitude of the uniform slip is 1 m (Mw ≈ 6.2). Results were computed with the PEGRN/PECMP code (Wang and Kümpel, 2003) at a depth of 500 m.

permeability changes induced by the earthquakes (e.g. Brodsky et al., 2003; Geballe et al., 2011), undrained consolidation and compaction of unconsolidated sediment (e.g. Marema et al., 2023; Nespoli et al., 2016; Wang et al., 2001). As suggested by Nespoli et al. (2016) which used the TOUGH2 code to model the evolution of pore-pressure after an earthquake, also the alternation at depth of rock layers having different poro-elastic parameters can significantly affect the behavior of the water level changes.

The post-seismic poro-elastic response (e.g. Bosl and Nur, 2002; Peltzer et al., 1998; Segall, 2010) can be modeled analytically under simplifying assumptions of a fully saturated, homogeneous poro-elastic medium (e.g. Piombo et al., 2005). Piombo et al. (2005) study the different effects of a poro-elastic response in presence of a permeable or impermeable fault. The co-seismic and one-year post-seismic displacements generated by three faulting cases with uniform slip (Normal, Thrust and Strike-Slip) are shown in Fig. 6. We can note that the post-seismic displacement magnitude is lower with respect to the co-seismic one, but not negligible.

4.4. Poro-elastic heterogeneities

The assumption of a uniform permeability value for the whole crust is unrealistic, since a progressive (logarithmic) decrease of crustal permeability with depth is generally expected (Ingebritsen and Manning, 2010). Scibek (2020) published a very detailed database reporting permeability values of fault zones at different geographic sites. In some studies, permeabilities are estimated directly, by applying the Darcy Law (Eq. (3)) to a rock sample in the laboratory, in other cases the estimates are indirect (e.g. observation of the seismicity migration over time, calibration of numerical models of fluid flows and Geochemical/mineralogical methods). The presence of layers with different elastic parameters affects the deformation field induced by a seismic fault (e.g. Nespoli et al., 2017). To model the layered medium, an effective semi-analytical approach is the one proposed by Wang and Kümpel (2003) and implemented in their code PEGRN/PECMP. Nespoli et al. (2018) used this code to effectively model the 3D poro-elastic response of the 2012 M6.1 Emilia-Romagna earthquake (Italy). The modeled response was then compared to the ground displacement data measured with Interferometric Synthetic Aperture Radar (InSAR) and Global Positioning System (GPS) observations. They found that a fast (≈ 1 week) post-seismic response was likely due to the poro-elastic fluid flow occurring in the highly permeable shallowest layers. A much slower trend of the poro-elastic response (≈ 1 year) instead can be linked to the slow fluid flow occurring at greater depths, which are characterized by a smaller permeability. Similarly, for the Nicoya (Costa Rica) Mw 7.6 earthquake of 2012, McCormack et al. (2020) found that the poro-elastic deformation measured by some GPS stations can account for most of the postseismic deformation occurred in the first 7 days following the mainshock. More recently, the PEGRN/PECMP code was also used by Yang et al. (2022) to model the poro-elastic response to the Mw 8.3 Illapel (Chile) megathrust event that occurred in 2015. To include more complex heterogeneities of the medium, FEM can be applied (e.g. Hughes et al., 2010). For example, Albano et al. (2017) used a 2D FEM section to model the poro-elastic response of the M 6.1 Emilia-Romagna earthquake (Italy) of 2012. They suggest that the post-seismic, poro-elastic effects can induce afterslip even on the main fault, thus favoring further seismicity.

4.5. Fluid-related effects on faults

During the post-seismic phase, the fluid flow can in turn generate deformation and trigger seismicity according to the Eq. (22). Peikert et al. (2022) investigated the relative importance of poro-elastic and visco-elastic postseismic relaxation using a 2D FEM for dip-slip faults. Faults are assumed to be located above the viscoelastic lower crust and lithospheric mantle. They suggest that both poro-elastic and visco-elastic effects overlap and should be considered to correctly interpret the post-seismic geodetic data and the aftershock distributions in terms of postseismic Coulomb stress changes. After an earthquake, either in the early stages or on long time scales, both processes can be relevant, depending on the assumed viscosity values and permeability values. If the permeability is low enough, poro-elastic effects cannot be neglected on time scales of years (Nespoli et al., 2018; Peikert et al., 2022). Deformation is affected by pore pressure changes in the near-field, whereas viscoelastic effects are important even in the far-field (Freed et al., 2006; Mandler et al., 2021; Peikert et al., 2022).

Fluid diffusion following a mainshock can contribute to the initiation and progression of aftershocks and complex seismic sequences (Chiarabba et al., 2020; Parotidis et al., 2003; Zhao et al., 2015). This occurs because fluid flow leads to the gradual redistribution of pore pressure, decreasing the strength of the rock over time, and potentially causing delayed fracturing (Nur and Booker, 1972). Moreover, coseismic changes in permeability can create preferential pathways for fluid diffusion, which may trigger multi-mainshock seismic sequences (Malagnini et al., 2022). Changes in seismicity rates can also be explained as a consequence of fluid diffusion (Hainzl and Ogata, 2005).

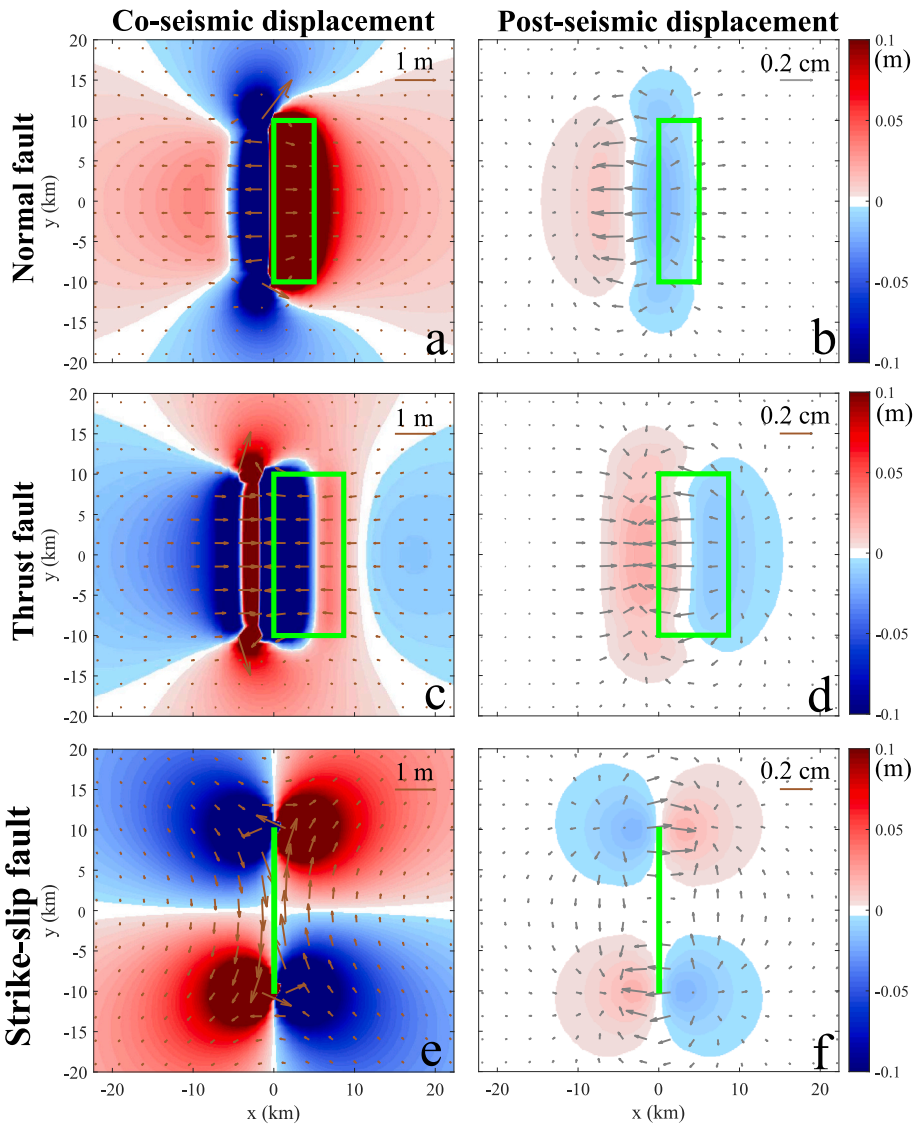

Fig. 6. *Co*-seismic (a, c and e) and 1-month Post-seismic displacement (b, d and f). The post-seismic displacement is computed as $\mathbf{u}^{PS}(t) = \mathbf{u}(t)$ - $\mathbf{u}(t = 0)$, where $\mathbf{u}(t = 0)$ is the co-seismic one. Vertical (color) and horizontal (arrows) components computed at the surface for a Normal (a, b), Thrust (c, d) and a left lateral Strike-slip fault (e, f). The top of the faults is 1 km, the length is 20 km and the width is 10 km. The strike is 0°N for all faults. The dip is 60° for the normal fault, 30° for the thrust fault and 90° for the strike-slip fault. The green lines indicate the fault traces. The poro-elastic parameters are pertinent to describe the Ruhr sandstone (Wang, 2000): μ =13 GPa, $\upsilon = 0.12$, $B = 0.88$, $D = 5.3{\cdot}10^{-3}$ m^2/s, $\alpha = 0.65$. The magnitude of the uniform slip is 1 m. Results were computed with the PEGRN/PECMP code (Wang and Kümpel, 2003). (For interpretation of the references to color in this figure legend, the reader is referred to the web version of this article.)

The importance of the fluid diffusion during a seismic sequence can be evidenced by observing the migration of seismicity which in some cases follows a diffusive behavior (see Figs. 2 and 3 of Antonioli et al., 2005), similarly to what is observed in EGS. The mechanism of seismicity triggering can be represented as well following the criterion presented in Section (2.4): the fluid flow which occurs after an earthquake leads to a redistribution of the pore-pressure and a change of the Coulomb stress which can favor seismicity in the proximity of the fault. For example, Kariche et al. (2018) found that poro-elastic relaxation and stress transfer are suitable to explain the triggering of post 1944 *Al* Hoceima (Morocco) earthquakes. Antonioli et al. (2005) found that the observed spatio-temporal migration of the 1997 Umbria-Marche (Italy) seismic sequence is consistent with fluid flow diffusion. Other interesting examples come from some African earthquakes (Kariche and Meghraoui, 2021) and the 2001 Mw 7.7 Bhuj (India) earthquake (Mandal et al., 2016). Convertito et al. (2013) suggested that the evolution of the 2012 Emilia (Italy) seismic sequence can be explained considering the dynamic triggering due to the passage of the seismic waves, together with the variations of permeability and pore-pressure increases in zones with massive presence of fluids. For the 1997 Umbria-Marche seismic sequence (Italy), Miller et al. (2004) found that both co-seismic and post-seismic responses were driven by a pressure pulse of CO_2 released by a deep reservoir. For the 2020 Westmorland (California) earthquake swarms, Sirorattanakul et al. (2022) found that up to 30 % of the seismicity was probably due to the pore-pressure diffusion.

For the purpose of clarifying the mechanism of possible hydrological precursors to earthquakes (e.g. Roeloffs, 1996; Yu et al., 2023), the National Institute of Advanced Industrial Science and Technology (AIST) in Japan is monitoring groundwater levels in observation wells (Itaba et al., 2010). Tokai region, a central part of the Honshu (Main Island), is considered to be the area where a devastating earthquake, the Tokai Earthquake, may occur. Observation of groundwater, especially groundwater level, is regarded as useful for forecasting earthquakes. AIST monitored groundwater in the Tokai region since 1976 and is responsible for groundwater observation in the Tokai region (https://gbank.gsj.jp/wellweb/GSJ_E/index.shtml). After the 1995 Hyogo-ken

Nanbu Earthquake (Kobe Earthquake), AIST set up an observation network composed of about 30 wells, mainly along active faults in and around the Kansai area, for the monitoring of active faults or research for the prediction of inland earthquakes. Some preseismic changes in groundwater level and crustal strain, which can be explained by accelerated pre-slip on the earthquake source fault or another nearby fault, have already been observed. The quartz-type pressure gauge sensor for the groundwater level meter is set about 5 m under the water surface. The temperature sensor is set at screen depth. Observation data of groundwater level is compared with barometric pressure, rainfall, and temperature. Similar networks have been set up in USA by USGS (https://www.unavco.org/data/strain-seismic/pore-pressure-data/pore-pressure-data.html), in Taiwan (Liu et al., 2023) and in China (Huang et al., 2017; Wang et al., 2018).

5. Volcanic regions and TPE inclusions

Volcanic regions are important study areas for testing and applying the models of fluid diffusion within the Earth's crust. The ascent of magma that occurs in volcanic regions is generally accompanied by the exsolution (Sigurdsson, 2000) of volatiles (mainly H_2O, CO_2, SO_2 and H_2S) which, after being released during magma depressurization (e.g. Belardinelli et al., 2022), rise towards the Earth's surface. This occurs because when ascending magma reaches the shallow crust it is subjected to a much lower lithostatic pressure, so it loses pressure and releases gasses. The presence of hydrothermal fluids is revealed at the surface through gaseous emissions such as the fumaroles.

Effective modeling of volcanic deformation includes assuming magma-filled sources embedded in elastic media (Bonafede et al., 2022; Mogi, 1958; Trasatti et al., 2011; Yang et al., 1988), or accounting for the TPE mechanical effects of magmatic fluids propagation in the hydrothermal system (e.g. Rinaldi et al., 2010; Todesco, 2021; Belardinelli et al., 2019; Currenti et al., 2024). Magma-filled sources are used to represent magmatic intrusions in rock layers, such as dikes (near-vertical intrusions) and sills (horizontal intrusions), as well as magma chambers (reservoirs). In principle, the TPE model might also extend to the uprise of highly viscous magmatic fluids, as this scenario still involves heat advection through mass movement driven by a pressure gradient. However, the predominant mechanism for magma uprise is typically ascribed to the upward propagation of magma-filled tensile fractures to model the dike ascent, a process that Darcy's law cannot adequately explain.

Modeling the hydrothermal system of a volcano is crucial both scientifically and for assessing volcanic hazards. Accurate models help interpret signs of volcanic unrest and predict potential pre-eruptive activities, improving our ability to estimate and manage risks in volcanic regions. Volcanic unrest is a phase during which a volcano shows signs of increased activity, such as more frequent earthquakes, soil deformation, higher gas emissions, or rising temperatures. While unrest can potentially lead to an eruption within a short timeframe (ranging from days to months) it does not always result in one. If an eruption does occur, it could either involve magma or be primarily driven by the expansion of steam and hot water (hydrothermal fluids) without magma reaching the surface (Gottsmann et al., 2017).

Behind magmatic eruptions, *phreatic eruptions* can be also very dangerous. They are due to the sudden expansion of steam heated by magma that can generate strong explosions accompanied by the expulsion of ash and rock fragments and the release of hydrothermal fluids. A particularly dramatic case was the 2014 phreatic eruption of Mt. Ontake (Japan), which resulted in the deaths of 63 hikers. Unfortunately, precursory ground deformation is not always observed before a phreatic eruption. One case study that represents an interesting exception is the 2018 phreatic eruption of the Iwo-Yama volcano (Japan). Between 2014 and 2016, ground inflation showed an axisymmetric pattern, with the greatest displacement occurring at the center of the deformed area. However, from 2016 the inflation became more concentrated and was located near the newly formed vents in the 2018 eruption (Narita et al., 2020): to explain these observations the authors infer the presence of two different shallow deformation sources, the first of which began to pressurize in 2014 and the second starting from 2016. Recently, Flóvenz et al. (2022) found that the cyclical injection of magmatic fluids released into the shallow hydrothermal system, during the ascent of magma, can explain both the inflation/deflation and seismicity cycles with periods of several months observed in Fagradalsfjall (Iceland). They also suggest that such cyclical behaviors can be interpreted as a precursor to the 2021 Fagradalsfjall magmatic eruption. The importance of forecasting phreatic eruptions highlights the need to develop models capable of representing the mechanical effects induced by the hydrothermal system. These effects are significant and should not be overlooked, making this line of research essential for further research (Mannen et al., 2019).

5.1. Hydrothermal fluid raising

The flow of hydrothermal fluids can be very complex to model since within the same system, different chemical species, phases, degrees of saturation of the pores and high pore-pressure and temperature gradients can coexist. Moreover, there may be heterogeneities of the medium which favor complex patterns of the fluid's circulation. In this scenario both the theories of permeable media (Section 2.1) and poro-elasticity (Section 2.2) can be applied effectively. However, due to the high temperatures at which magmatic fluids may be found, it is often necessary to extend the poro-elasticity to the thermo-poro-elasticity (Section 2.3). In this line, Zencher et al. (2006) proposed a 1-D TPE model to represent the fluid rising through a transition layer (Fig. 7) located between a shallow meteoric aquifer with a pore-pressure in *hydrostatic conditions* ($p = \rho_f g z$) and a deeper reservoir with a higher

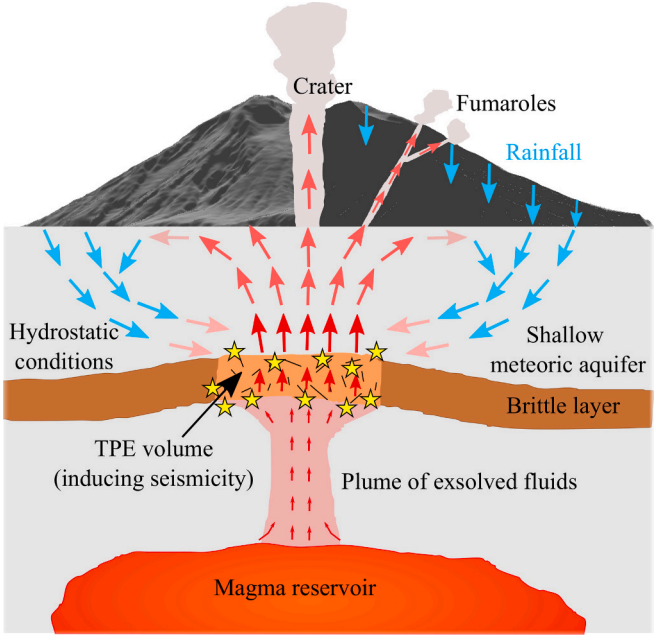

Fig. 7. Sketch of a generic hydrothermal system with a TPE deformation source located below a volcano. The plume of hot and pressurized fluids exsolved by a deep magma reservoir (red) crosses a brittle layer (brown) that separates the shallow meteoric aquifer from the deepest part of the system. During the unrest phases the stress induced by the deep magmatic reservoir can fracture a portion (orange) of the brittle layer which increases its permeability. The fracturing of the layer allows the ascent of fluids from the deep system to the shallow meteoric aquifer. The mechanical effects and the induced seismicity generated by the flow of the hot and pressurized fluids within the brittle, fractured volume can be represented with a TPE inclusion model. (For interpretation of the references to color in this figure legend, the reader is referred to the web version of this article.)

pore-pressure in *lithostatic conditions* ($p = \rho_s gz$). Hydrostatic and lithostatic conditions describe scenarios where the pore-pressure at a given depth, z, is due to the weight of the overlying fluid or rock, respectively. Their model could be applicable to various volcanic areas, such as the South Iceland seismic zone.

The TOUGH2 code (Pruess et al., 2012) was effectively used to model the complexities of multiphase and multicomponent hydrothermal fluids in several regions such as the Vulcano Island (Italy) (Currenti and Napoli, 2017), the White Island (New Zealand) volcano (Fournier and Chardot, 2012), the Campi Flegrei (Italy) caldera (Chiodini et al., 2003; Rinaldi et al., 2010; Todesco et al., 2003; Todesco and Berrino, 2005) and the Poás (Costa Rica) volcano (Todesco et al., 2015). Usually, the modeling phase starts from creating a 2D or a 3D mesh-grid which is suitable to represent the geometry and the main geological features of the study area. Then the *steady state* of the model must be reached imposing the steady state boundary conditions. From the steady state, a perturbation of the system can be introduced. Such a perturbation is realized with new boundary conditions (e.g. higher pore-pressure or temperature at the bottom of the model) or the input/output of fluids. In both cases it is possible to study in detail the propagation of fluids within an initially unperturbed system, as could happen during the migration of a plume of hot and pressurized fluids, released from a deeper magma chamber.

The HYDROTHERM simulator (Kipp et al., 2008), which allows us to model heat transport and multiphase ground-water flow in 3D, is also widely used in the volcanological field (e.g. Hsieh and Ingebritsen, 2019; Reynolds et al., 2017). With respect to the standard TOUGH2 code, which is restricted to temperature $T < 350$ °C and pore-pressure lower than $p < 100$ MPa, the HYDROTHERM simulator can reach much higher pore-pressures and temperatures ($T < 1200$ °C and $p < 1000$ MPa). For this reason, HYDROTHERM is more suitable to model high-energy hydrothermal systems such as deep geothermal reservoirs or hydrothermal systems hosting magmatic fluids exhaled from a deep magma chamber whose temperature can easily be above 350 °C (Ikeuchi et al., 1998). This limit corresponds approximately to the critical point temperature of water ($T = 373.946$ °C) near which, the physical properties of the liquid and vapor undergo significant changes, causing the two phases to become increasingly similar. This can create problems both in the convergence of the solutions, in the calculation of the mass balance and in the assignment of the fluid saturation, which, for example, is a dependent variable in TOUGH2. Another option is the non-commercial multiphase and multicomponent fluid flows (MUFITS) (Afanasyev, 2012) which can model fluids in supercritical conditions (maximum $p < 150$ MPa and $T < 1000$ °C). It must be recalled that to model the deformation associated with hydrothermal fluids, these simulators alone are not sufficient. They must be coupled with other softwares. For example, the coupling between the TOUGH2 with BIOT2 software (Hsieh, 1996) was used by Hurwitz et al. (2007) to model fluid flow and deformation in calderas. In the same line, Coco et al. (2016) coupled a finite-difference ghost-point method with TOUGH2 to simulate the hydrothermal system dynamics of a restless caldera.

5.2. TPE inclusions

Another recent approach to model TPE effects due to magmatic fluids involve the TPE inclusions (Eshelby, 1957), representing limited volumes of rocks which undergo variations of pore-pressure and temperature, embedded in a poro-elastic medium in drained and isothermal conditions. Even if TPE inclusion models were firstly used to model the effect of the injection and withdrawal of fluids associated with the exploitation of geothermal resources, as reported in Section (3.1), more recently they were successfully applied to model the deformation/stress and the seismicity in volcanic regions. In such a scenario the pore-pressure and temperature changes occurring inside the TPE inclusion do not derive from the well injection/production but from the exsolution of fluids of magmatic origin.

According to Belardinelli et al. (2019) the mechanical effects of a TPE inclusion can be computed by rewriting Eq. (15) as:

$$e_{ij} = \frac{1}{2\mu}\left(\tau_{ij} - \frac{\nu}{1+\nu}\tau_{kk}\delta_{ij}\right) + e_0\delta_{ij} \tag{27}$$

where the TPE *inclusion potency* e_0 is defined as:

$$e_0 = \frac{1}{3H}p + \frac{1}{3}\alpha_s T \tag{28}$$

The importance of e_0 stems from the fact that it determines the magnitude of all the mechanical effects (displacement, strain and stress) generated by a TPE inclusion as a deformation source. In fact, the displacement can be computed integrating over the volume V_S of the inclusion as:

$$u_i = 3Ke_0 \int_{V_s} \frac{\partial G_{ik}}{\partial x_k'}\left(\mathbf{x}, \mathbf{x}'\right) dV' \tag{29}$$

where G_{ik} is the Green's tensor for a half-space in isothermal and drained conditions and indicates the displacement in the i-th direction at **x** due to a unitary force acting in the k-th direction located at **x'**. The stress inside the source can be computed as:

$$\tau_{ij} = \lambda\epsilon_{kk}\delta_{ij} + 2\mu\epsilon_{ij} - 3K\epsilon_o\delta_{ij} \tag{30}$$

while outside the inclusion it is

$$\tau_{ij} = \lambda\epsilon_{kk}\delta_{ij} + 2\mu\epsilon_{ij} \tag{31}$$

In a full space, the mechanical effects of TPE inclusions were computed analytically from Eq. (29) for spherical and spherical shell inclusions by Belardinelli et al. (2019) and for thin disk inclusions by Belardinelli et al. (2022). Semi-numerical approaches allow representing the free surface (Mantiloni et al., 2020), while pure numerical approaches based on the EFGRN/EFCMP software (Nespoli et al., 2021a, 2022) allow modeling complex TPE geometries embedded in layered media. The usefulness of TPE inclusions (Nespoli et al., 2023a) is due to the fact that they create a strong deviatoric stress field (favoring the seismicity) within them. In fact, different from TPE inclusions, the models commonly used to represent pressurized magma cavities have zero shear stress inside, therefore they do not justify the presence of earthquakes inside them. TPE inclusions can be also used to explain deformations even in volcanic environments without evidence of the presence of shallow magmatic bodies (Nespoli et al., 2021a). Moreover, they are suitable to model the heterogeneity of fault mechanisms occurring within and around them (Fig. 8a and b). Resulting displacement and stress due to a disk-shaped TPE inclusion are reported in Fig. 8c which shows a strong concentration of the induced shear stress close and within the TPE inclusion volume, where it can favor the occurrence of earthquakes.

Most recent applications of TPE deformation sources regard the Campi Flegrei (Italy) caldera, a well-studied and monitored volcano, with an important role in terms of geohazard. Here an uplift up to 1.8 m was observed close to the center of the caldera during the unrest period from 1982 to 1984 (Del Gaudio et al., 2010). Subsequently, there were 20 years of subsidence. Then, in 2005 a new uplift phase started and it is still going on. Both the 1982–1984 and the current unrest phases were accompanied by an increase of the seismicity rate and the fumarole activity (Tramelli et al., 2021).

Different models were employed to model the deformation at Campi Flegrei (see Bonafede et al. (2022) for a review of them). In addition to these, Mantiloni et al. (2020) and Nespoli et al. (2021a) showed how a disk-shaped TPE inclusion model can effectively explain both the observed deformation and seismicity. Starting from the equations of section (5.2), Belardinelli et al. (2022) and Nespoli et al. (2021a) also reported the analytical TPE solutions which can be used to represent the vertical propagation of hot and pressurized fluids rising from the bottom

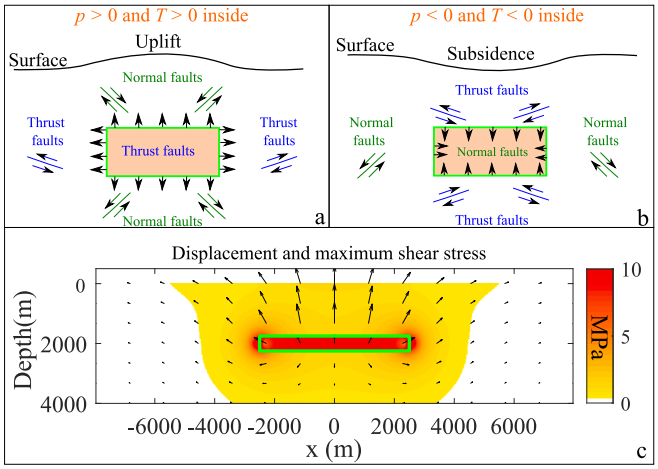

Fig. 8. Sketches of TPE inclusions (orange volume) for (a) increments and (b) reduction of pore-pressure p and temperature T inside. The zones in which fault mechanisms (thrust or normal faults) are favored in the two cases are also reported. Black arrows illustrate the direction of the displacement in the TPE inclusion boundaries (not in scale). Panel (c) shows the computed displacement (black arrows, exaggerated by a factor 1000) and the maximum shear stress (color) generated by a test case TPE inclusion (Radius = 2.5 km, depth = 2 km, width = 0.5 km) undergoing positive changes of $p = 10$ MPa and $T = 100$ K. For the computation, we use $\mu = 6$ GPa and $\nu = 0.2$ ($K = 8$ GPa), $H = 10$ GPa, $\alpha_s = 3\times$ 10–5 K − 1. Fields computed with the EFGRN/EFCMP code (Nespoli et al., 2022).

to the top of a disk-shaped TPE inclusion embedded in a full space or in a half space, respectively. Their solutions are suitable to model magmatic fluids released by a deep magmatic chamber across a shallower TPE volume during their rise to the Earth's surface and were obtained under the simplifying assumption of uniaxial strain, constant vertical stress, and constant permeability. Such solutions were applied to model the current unrest phase occurring at Campi Flegrei by Nespoli et al. (2023b).

Both spherical and cylindrical TPE inclusions were recently used to model the observed axi-symmetric inflation pattern (with a maximum uplift of 1.3 cm occurred in 2021) at the Vulcano Island, Italy, by Stissi et al. (2023). By assuming that the deformation was only driven by the pore-pressure, they found that a pore-pressure increase between 0.01 and 7 MPa, occurred inside a TPE source located at a depth of about 800 m, can suitably explain the observations. Even in this case they hypothesize that the hot and pressurized fluid flow originated from a deeper degassing magma chamber.

6. Additional application areas of poroelasticity

Within the broader scope of geoscience and engineering applications where poroelasticity has a key role, the following areas are particularly noteworthy:

- *Nuclear waste geological storage:* the disposal of nuclear waste in the underground is a viable option for the high-level waste (HLW) produced at nuclear power plants (e.g.,https://nagra.ch/en/why-nagra/). Disposal of radioactive material requires a low permeability formation, in which several tunnels are excavated to be filled with specifically engineered canisters containing the HLW and buffer material, such as sand and bentonite (Sellin and Leupin, 2013). In the first 1000 years after the emplacement of the nuclear waste, the thermal perturbation caused by radioactive decay represents the driving mechanism within the repository (NAGRA, 2016). The generated heat dissipates through the buffer material and the host rock, causing steam convection in the de-saturated repository near-field. This region is slowly re-saturated by inflow from the low permeable host rock. Another thermo-hydraulic process that occurs in geological nuclear waste disposal is the so-called thermal pressurization: a pressure build-up resulting from differential thermal expansion that could potentially trigger mechanical processes (Nguyen, 2018; Tsang et al., 2012). Despite the potential to induce few MPa changes in pressure, the thermal pressurization does not have hydrological relevance, due to the low permeability of the hosting rock; however, the consequent increase in pressure could induce significant geomechanical variations through poroelastic effects, including induced seismicity in the underlying formations (Urpi et al., 2019). Such changes may also be relevant in the post-closure phase, which could feature, from the poro mechanical perspective, processes due to the long-term deformation behavior.
- *Underground laboratory experiments:* several facilities around the world are focusing their effort in performing experiments at in-situ conditions. Examples are the laboratories in Switzerland (Grimsel, e.g. Amann et al., 2018; Mont Terri, e.g. Bossart et al., 2017; Bedretto, e.g. Ma et al., 2022), France (Tournemire, e.g. De Barros et al., 2018; LSBB, e.g. Guglielmi et al., 2015) and US (Surf, South Dakota, e.g. Kneafsey et al., 2022; Schoenball et al., 2020). Underground laboratories can provide access to natural conditions at several hundred meters depth, helping better represent the state-of-stress. Several of these experiments, performed at LSBB and Mont Terri (Cappa et al., 2019, 2022; Guglielmi et al., 2015, 2021; Hopp et al., 2022; Zappone et al., 2021) have clearly shown how the fault reactivation and the seismicity are influenced by poro-elasticity. The main observations are explained by poro-elastic clamping of the injection region and shear stress generated by aseismic slip at the limit of the pressurized area, eventually resulting in seismicity (Cappa et al., 2019). A recent paper by Dutler et al. (2021) also shows how pore pressure changes due to injection in a fractured network can be seen through undrained poro-elasticity at distances of more than 100 m far beyond the region affected by induced seismicity.
- *Tectonics and Seismic cycle:* Tectonic deformation and the presence of fluid are the basic, intrinsic processes that lead to earthquake nucleation and rupture. Several studies have recognized the fluids as essential in tectonic processes (Miller, 2013; Saffer and Tobin, 2011). The most relevant fluid is water that could be released by dehydration reactions that could cause pore pressure changes especially in the presence of low permeability asperities barriers (Audet et al., 2009; Gao and Wang, 2017). The breaching of these barriers is referred to as a fault-valving model (Sibson, 1990; Zhu et al., 2020). More recently, the inclusion of fluid pressurization and poro-elasticity has become widely spread. Effects such as strength reduction due to pore-pressure increase, poro-elastic effects on rate-strengthening, and pressurization due to shear heating can all in a way promote aseismic or dynamic failure (Heimisson et al., 2019; Ikari et al., 2013; Noda and Lapusta, 2013; Rice, 2006; Scholz, 1998; Segall and Rice, 1995; Sibson, 1973), while theoretical frictional consideration and dilatancy effects during fault slip could promote fault stability (Dal Zilio et al., 2020; Dieterich, 2007; Liu and Rubin, 2010; Marone, 1998; Segall and Rice, 1995). Recently, modeling effort further highlighted that a wide range of behavior can develop from the choice of the hydraulic properties and their evolution in a fault zone (Dal Zilio and Gerya, 2022) and that poro-elastic coupling on a finite-width shear fault can further promote failure (Dal Zilio et al., 2022).

7. Discussion and conclusions

In this work we have reviewed some of the most important applications of crustal fluids models in geophysics. In particular, we have focused attention on three main topics that can be treated with sufficient accuracy following the linear theories briefly introduced in Section 2: resources exploitation and its link to induced seismicity (including geothermal, hydrocarbon injection/production, and reservoir induced

seismicity), relationship between faults and fluids, and hydrothermal systems in volcanic fields. Table 1 outlines the models, theories, and applications associated with porous media, while Table 2 reports the main characteristics of the key articles employing different modeling approaches.Table 3 reports a list of the presented thermo-poro-elastic parameters with their units of measure.

7.1. Near future directions in different fields of applications

Regarding resource exploitation and the related induced seismicity, in addition to the economic interest that concerns the optimization of the process, a main objective is to estimate the seismogenic potential of the anthropic activity on a given system. In order to achieve this purpose and have a correct representation of the phenomenon, we need models suitable to reproduce with extreme precision fluid diffusion and poro-elastic stresses. Near an injection well induced poro-elastic stresses can be relevant even outside the region where pore-pressure changes can induce seismicity (Ge and Saar, 2022). Both mechanisms together with static Coulomb stress transfer can increase seismicity rates. The recent literature suggests that these three mechanisms operated concurrently (or consecutively) at most induced sites (Ge and Saar, 2022). The future directions of this research topic require the development of coupled models that can represent all these phenomena in parallel.

The importance of accurately modeling the poro-elastic effects due to an earthquake is made evident by some recent studies which suggest that to discern the different contributions in the post-seismic signal, the poro-elastic ones cannot be neglected. According to Peña et al. (2022) the spatial distribution of afterslip inferred by neglecting poro-elastic effects can be locally altered by up to ±40 %. In the same line McCormack et al. (2020) suggested that inversions for the retrieval of afterslip that neglects poro-elastic effects can induce errors of 10–20 % overall and up to 50 % locally. These results indicate to us that unlike what is commonly done today, in the future it could (and should) become routine to include poro-elastic effects in the inversion of geodetic data. Otherwise, an incorrect interpretation of the behavior of the seismic source would be obtained.

Even in volcanic environments, the thermo-poro-elastic theory can find ample space for application in the future. One of the most current scenarios in which the theory can be applied is the Caldera of the Campi Flegrei in Italy. The scientific literature is strongly divided on the interpretation of the bradyseism (deformation) phenomenon that has been affecting the area in recent years (Bonafede et al., 2022). End-member processes for the interpretation of the phenomenon are the rise of superficial magma or to thermo-poro-elastic effects induced by the shallow hydrothermal system. Probably, the correct interpretation must consider a superposition of magmatic and hydrothermal effects (De Siena et al., 2024; Nespoli et al., 2023b), but only by clarifying this point will it be possible to fully understand the state of the volcanic system and reach a correct geohazard assessment. For this reason, future studies in the volcanological field can greatly benefit from thermo-poro-elastic models. One of the possible advances in the volcanological field could consist in the development of hydrothermal system models that account for 3D geometries to explain the observed variations in the deformation field and fluid seepage on a small spatial scale. A three-dimensional representation of the hydrothermal system would also allow for more accurate modeling of the heterogeneous distributions of seismicity. The application and the development of more sophisticated fluid propagation models which account for different fluid species and phase changes can also improve the understanding of the functioning of a hydrothermal system. Moreover, in volcanic zones models can be complicated by the fact that due to the high temperatures, fluids can be in the supercritical state with different densities and viscosities compared to both liquid and gas phases. A further improvement of the poro-elastic and thermo-poro-elastic theories, especially in volcanic and geothermal environments, can be made by including the visco-elastic rheology (Acocella, 2021) of the solid matrix to obtain a thermo-poro-viscoelastic medium. This generalization can be important in cases of high temperatures and/or high pore pressure promoting thermally activated creep (Goetze and Evans, 1979) and pressure-solution creep, respectively (Gratier et al., 2013). A thermo-poro-viscoelastic medium can be represented starting from the thermo-poro-elastic solutions by using the correspondence principle (Fung, 1965) as done, for example, by Nespoli et al. (2023a).

The fields of application of the poro-elastic theory do not end with those presented in Sections 3 to 6 but find space in numerous geo-mechanical and geotechnical applications (see Wang, 2000). For example, poro-elasticity is also used to study the mechanical response to rainfall in aquifers that host the meteoric water (e.g. Alghamdi et al., 2020; Nespoli et al., 2021b; Woodman et al., 2019). Generally, the models illustrated in the present paper can find applications even in geodesy, studying crustal deformations caused by hydrological

Table 1
Overview of models, theories, code packages and applications related to poros-medium mechanisms.

Physical Mechanism	Key Features	Equations	Available Code Packages	Computing Complexity	Accuracy	Potential/Successful Applications
Poros (P)	Fluid flow in permeable media	Darcy's Law (Section 2.1)	HYDROTHERM, TOUGH2, TOUGH3, MUFITS and COMSOL	Moderate	High	Groundwater flow, oil and gas migration, pore pressure evolution
Poro-Elastic (PE)	Coupled fluid flow and elastic deformation	Biot's theory with drained/undrained conditions (Section 2.2)	- POEL (single phase and component of fluid), MODFLOW-2005, TOUGH-FLAC, TOUGH3-FLAC3D, - Analytical geodetic seismic response: PEGRN/PECMP, FEM - To include chemical reactions: TOUGHREACT, STOMP-EOR, and GEM	Moderate	High	Reservoir-induced seismicity, hydrocarbon exploitation, Hydrology and Environmental Engineering, co-seismic/post-seismic effects, fault pressurization
Thermo-Poro-Elastic (TPE)	Thermal effects on fluid and matrix	Extended Biot's theory with coupled thermal, hydraulic, and mechanical processes (Section 2.3)	- TOUGH2 (no mechanical coupling), ITOUGH2 (inversion), TOUGH2-seed, HYDROTHERM (heat transport and multi-phase fluid flow in 3D), - More advanced: COMSOL, TOUGH-FLAC, VISAGE, STARS	High	Moderate-High	Geothermal energy extraction, volcanic deformation, thermal subsidence.
Thermo-Poro-Viscoelastic (TPVE)[1]	Application in highly dynamic and thermally active environments	Comprehensive coupling of thermal, hydraulic, mechanical, and visco-elastic rheology	Analytical	High	Moderate-High	High temperatures and/or high pore pressure promoting thermally activated creep and pressure solution creep; Complex geothermal systems, advanced earthquake research,

[1] Not a focus of this paper.

Table 2
List of key articles employing different modeling approaches. P = porous, PE = Poro-Elastic; TPE = Thermo-Poro-Elastic; VE = Visco-Elastic; TPVE = Thermo-Poro-ViscoElastic; Var = variable permeability and/or porosity. *SUTRA, Saturated-Unsaturated TRAnsport; (Voss and Provost, 2002). **(MSC, 2015). ***OGS (Benisch et al., 2020), ****ABAQUS, https://www.3ds.com/products/simulia/abaqus.

Article	Zone	Model	Medium
Resources exploitation			
Geothermal			
Catalli et al., 2016	EGS of Basel, Switzerland	COMSOL + stochastic model	P
Rinaldi and Nespoli, 2017	EGS of Basel, Switzerland	TOUGH2 + stochastic model	P + Var
Liu et al., 2020	Guide basin, China.	TOUGH2	P
Yuono and Daud, 2020	Flores Island, Indonesia	TOUGH2 and ITOUGH2	P
Zeng et al., 2013	Desert Peak, Nevada, USA	TOUGH2-EOS1	P
Gischig and Wiemer, 2013	EGS of Basel, Switzerland	COMSOL+ stochastic model	P + Var
Ritz et al., 2020	Different scenarios	TOUGH2 + stochastic model	P + Var
Zbinden et al., 2020a	*St.* Gallen Deep Geothermal Project (Switzerland)	TOUGH2 + stochastic model	P + Var
Geertsma, 1973	Different scenarios	Analytical	PE
Rudnicki, 1999	Theoretical scenarios	Analytical	TPE
Segall, 1992	Lacq gas field, France	Analytical	PE
Guido et al., 2015	Lacq, France; Lombardia, Italy	Analytical	PE
Segall, 1989	Different scenarios	Analytical	PE
Segall and Fitzgerald, 1998	Geysers steam field, California, USA	Analytical	TPE
Segall and Lu, 2015	Theoretical scenarios	Analytical	PE
Deng et al., 2020	Western Texas, USA	POEL and MODFLOW	PE
Silverii et al., 2021	Southern Europe - Confidential	POEL	PE
Yu et al., 2019	Montney Basin, British Columbia	POEL	PE
Oil/Gas injection and production			
Rinaldi et al., 2017	In Salah, Algeria	TOUGH-FLAC	TPE
Rinaldi and Rutqvist, 2013	In Salah, Algeria	TOUGH-FLAC	TPE
Rinaldi et al., 2014	Theoretical scenarios	TOUGH-FLAC	TPE
Vilarrasa et al., 2017	In Salah, Algeria	TOUGH-FLAC	TPE
Zbinden et al., 2017	Different scenarios	TOUGH-FLAC	TPE
Smith et al., 2022	Groningen gas reservoir, Netherlands	Semi-analytical	PE
Kutsienyo et al., 2021	Farnsworth Unit, Texas, USA	TOUGHREACT, STOMP-EOR, and GEM	P + Var
Dam-reservoirs			
Büyükakpınar et al., 2021	Atatürk Dam, Turkey	Analytical	PE
Ruiz-Barajas et al., 2019	Pirrís Reservoir (Costa Rica)	Analytical	PE
Brothers et al., 2011	Salton Sea (California)	Analytical	PE
Durá-Gómez and Talwani, 2010	Itoiz Reservoir (Spain)	Analytical	PE
Ge et al., 2009	Zipingpu Reservoir (China)	MODFLOW	PE
Hill et al., 2023	Salton Sea (California)	Custom FEM	PE
Rinaldi et al., 2020	Pertusillo Lake (Italy)	Semi-analytical	PE
Hua et al., 2013	Longtan reservoir (China)	Analytical	P
Seismic faults and fluids			
Roeloffs, 1996	Alaska and China	Different	PE
Deng et al., 2016	Central Alberta, Canada,	Custom FEM	PE
Peltzer et al., 1998	Landers, California, USA	Analytical	PE
Ge and Stover, 2000	Theoretical scenarios	Analytical	PE
Jónsson et al., 2003	South Iceland seismic zone	Analytical	PE
Nespoli et al., 2016	Emilia romagna, Italy	TOUGH2	P + Coseismic PE
Akita and Matsumoto, 2004	Hokkaido, Japan	Elastic solutions by Okada (1992)	Coseismic PE
Brodsky et al., 2003	Grants Pass, Oregon, USA	Analytical	P + Var
Geballe et al., 2011	Wenchuan, Taiwan	Analytical	P + Var
Wang et al., 2001	Chi-Chi, Taiwan	Analytical	Var
Marema et al., 2023	Moiyabana, Central Botswana	Analytical	P
Bosl and Nur, 2002	Landers, California, USA	Custom numerical	PE
Piombo et al., 2005	Theoretical scenarios	Analytical	PE
Nespoli et al., 2018	Emilia Romagna, Italy	PEGRN/PECMP	PE
McCormack et al., 2020	Nicoya, Costa Rica	Custom FEM	PE
Yang et al., 2022	Illapel, Chile	PEGRN/PECMP	PE
Hughes et al., 2010	Sumatra–Andaman	Custom FEM	PE
Albano et al., 2017	Emilia Romagna, Italy	2D FEM (MSC Marc**)	PE
Peikert et al., 2022	Theoretical scenarios	2D FEM (ABAQUS****)	PE and VE
Antonioli et al., 2005	Umbria-Marche, Italy	Analytical	P
Kariche et al., 2018	Rif Mountains, Morocco and southern Alboran Sea	Analytical	PE
Kariche and Meghraoui, 2021	Different zones of Africa	Analytical	PE
Mandal et al., 2016	Bhuj, Gujarat, India	Analytical	P
Convertito et al., 2013	Emilia Romagna, Italy	Analytical	Var
Miller et al., 2004	Umbria-Marche, Italy	Analytical	P + Var
Sirorattanakul et al., 2022	Westmorland, California	Analytical	P
Volcanic regions and TPE inclusions			
Flóvenz et al. (2022)	Fagradalsfjall (Iceland)	POEL	PE
Zencher et al., 2006	South Iceland seismic zone	Analytical	TPE
Currenti and Napoli, 2017	Vulcano Island, Italy	TOUGH2 + COMSOL	TPE
Chiodini et al., 2003	Campi Flegrei, Italy	TOUGH2	P
Todesco et al., 2003	Campi Flegrei, Italy	TOUGH2	P
Todesco and Berrino, 2005	Campi Flegrei, Italy	TOUGH2	P
Rinaldi et al., 2010	Campi Flegrei, Italy	TOUGH2 + Analytical	TPE
Todesco et al., 2015	Poás volcano (Costa Rica)	TOUGH2	P
Hsieh and Ingebritsen, 2019	Kīlauea Volcano, Hawai'i	HYDROTHERM	P
Reynolds et al., 2017	Bárdarbunga-Holuhraun, Iceland	HYDROTHERM and COMSOL	P

(*continued on next page*)

Table 2 (*continued*)

Article	Zone	Model	Medium
Hurwitz et al., 2007	Campi Flegrei, Italy and Long Valley caldera, California, USA	TOUGH2-BIOT2	TPE
Coco et al., 2016	Campi Flegrei, Italy	TOUGH2 + Finite difference	TPE
Belardinelli et al., 2019	Theoretical scenario	Analytical	TPE
Belardinelli et al., 2022	Theoretical scenario	Analytical	TPE
Mantiloni et al., 2020	Campi Flegrei, Italy	Semi-Analytical	TPE
Nespoli et al., 2021b	Campi Flegrei, Italy	Custom numerical	TPE
Nespoli et al., 2022	Campi Flegrei, Italy	EFGRN/EFCMP	TPE
Nespoli et al., 2023a	Campi Flegrei, Italy	Analytical	TPVE
Nespoli et al., 2023b	Campi Flegrei, Italy	EFGRN/EFCMP	TPE
Stissi et al., 2023	Vulcano Island, Italy	Semi-Analytical	TPE

Table 3
List of parameters with their units of measure.

Symbol	Variable/parameter name	Unit of measure
p	Pore-pressure change	Pa
L	Cylinder length	m
A	Cylinder areal section	m^2
Q	Volume of fluids crossing section A	m^3/s
q	Darcy velocity	m/s
k	Permeability	m^2
η	Fluid viscosity	Pa s
ρ_f	Reference density of the fluid	kg/m^3
g	Gravitational acceleration	m/s^2
t	Time	s
Q_s	Source or sink	1/s
e_{ij}	Strain	–
τ_{ij}	Stress	Pa
ν	Poisson ratio	–
ν_u	Undrained Poisson ratio	–
B	Skempton's coefficient	–
μ	Rigidity	Pa
Δm	Mass content change/unit of volume	kg/m^3
P_c	Confining pressure	Pa
$1/H$	Poro-elastic expansion coefficient	1/Pa
K	Drained incompressibility	Pa
K'_s	Incompressibility of solid	Pa
α	Biot-Willis coefficient	–
T	Temperature change	°C
D	Hydraulic diffusivity	m^2/s
α_s	Thermal expansion of solid	K^{-1}
ρ_s	Density of solid	kg/m^3
c_s	Specific heat of solid	J / (kg K)
c_f	Specific heat of fluid	J / (kg K)
λ_s	Thermal conductivity of solid	J /(m K)
λ_f	Thermal conductivity of fluid	J /(m K)
f	Friction coefficient	–
f'	Effective friction coefficient	–
CFS	Coulomb failure stress	Pa
p_s	Pore-pressure change at the surface	Pa
γ	Loading efficiency	–
h	Water level height	m
e_0	TPE inclusion potency	–
G_{ik}	Green's tensor	m/N
Re	Reynold number	–
v	Seepage velocity	m/s
r	Characteristic dimension of grains	m

processes (D'Agostino et al., 2018; Pintori et al., 2021; Rossi et al., 2021). Strainmeters located near aquifers may record poro-elastic deformation which is in phase opposition with respect to the expected elastic deformation (Mandler et al., 2024; Segall et al., 2003). A future development of poro-elastic theory and models would also benefit these different applications which are very useful for the safe and sustainable development of society.

7.2. Limitations of the poro-elasticity due to non-linearities

The formulation of the Darcy (1856) law for permeable media followed by the poro-elastic theory of Biot (1941) and the thermo-poro-elastic theory of McTigue (1986) allow us to simplify the description of crustal fluid by macroscopic observations of processes that can occur at microscopic scales, within the pores of the rocks. Despite that, even the linear thermo-poro-elastic theory requires at least twelve parameters to describe the coupling between the rock matrix and fluids (Belardinelli et al., 2022). In some cases, however, it is necessary to introduce even more complex behaviors involving non-linear fluid-rock interaction (Bociu and Webster, 2021; Cao et al., 2013; Prévost, 1982, 1980; Segall, 2010; Viswanathan et al., 2022) as could occur in presence of permeability variation, fracture jacking and hydraulic fracturing. In the latter case the pore-pressure can be as high to overcome the tensile strength of the rocks leading to tensile fractures which increases the permeability of the medium. Moreover, non-linear behaviors can become important to some applications of geotechnical engineering (and also to biology) where the small deformation approximation is no longer acceptable. Other non-linear behaviors of poro-elastic materials can arise when the porosity and permeability of the medium depend on the divergence of the displacement, or dilation (Van Duijn and Mikelić, 2023).

Darcy's law provides an approximate description of fluid flow in porous media and is applicable only within a limited range of low velocities which depend on grain sizes. Experiments show that fluid flow can deviate from Darcy's law due to turbulent flows and inertial effects (Zeng and Grigg, 2006). One of the criteria that has been used to discriminate the transition between Darcy and non-Darcy flow is based on the Reynold's number (i.e the ratio of inertia force to viscous force of the fluid flowing in the porous medium), which is commonly used to estimate the transition between laminar and turbulent regime of a Newtonian fluid inside a cylindrical conduit. It can be expressed as $Re = \rho_f r v/\eta$ where r is a characteristic dimension of the grains and v is the real flow velocity. If the Reynolds number is greater than the critical value, which according to various studies is approximately between 0.1 and 100 (Zeng and Grigg, 2006), the fluid flow will be affected by high-speed nonlinearities.

7.3. Open problems asking for the development of more complex models

Developments of more complex models are required in a wide number of applications:

- Many real-world problems involve multiple coupled physical processes. For example, in geothermal reservoirs, (thermo-) poro-elasticity must be coupled with heat transport, chemical reactions, and multiphase flow. Thus, further development of multiphysics frameworks to incorporate thermal, chemical and electromagnetic (Markov et al., 2022) effects into poro-elastic models will certainly be important.
- Most existing poro-elastic models assume isotropy and homogeneity of the medium. However, many materials, such as composite materials and shale, exhibit anisotropic behavior (spatial heterogeneity), so the development of poro-elastic models that account for anisotropy in both the solid matrix and the fluid flow properties could be an important development of the theory (Carcione et al., 2011). The computational cost, especially for nonlinear, multiscale, or multiphysics problems, can be prohibitive and the development of more efficient numerical methods and the integration with machine learning and data-driven approaches can be important to improve the poro-elastic model predictions (Vasilyeva and Tyrylgin, 2021).

- Another line of the research should investigate further the role of poro-elasticity in the seismic cycle, as this is crucial for understanding earthquake mechanics and fault dynamics. Despite significant advancements, the precise mechanisms by which fluid pressure changes can trigger earthquakes remain not fully understood. As we have seen in the previous paragraphs variations in pore pressure can weaken fault strength, potentially leading to slip events. Under some assumptions it is possible to give an approximate representation of such processes but quantifying this effect remains a contemporary challenge (Dal Zilio et al., 2022)

In any case, the level of complexity of modeling crustal fluids can be very high, and one of the most intriguing challenges of geophysical research consists in finding the simplest model that can already represent the problem of interest, in terms of the basic physics regulating a certain phenomenon. Even if the capabilities of computers have greatly increased in recent decades, thus allowing for great improvements of the models, the introduction of too many complexities are not always necessary to explain the available data, and the risk of over-interpreting the modeling results is high. Moreover, a model that requires the definition of many parameters could be under-determined and may lead to a misinterpretation of the results. For this reason, it is important to continue developing both analytical and numerical models in the current state of research. On the one hand the analytical approaches which allow solutions in closed form (despite physical and mathematical simplifications) have a very important role in testing and validating more complex numerical models. On the other hand, numerical approaches allow us to study problems which are too complex to be solved analytically. Surely, the continuous evolution and comparison between analytical and numerical models is an effective approach to continue research in this topic.

Declaration of competing interest

The authors declare that they have no known competing financial interests or personal relationships that could have appeared to influence the work reported in this paper.

Acknowledgments

The authors would like to thank the Editor and the reviewers for constructive comments. The authors extend their heartfelt gratitude to Professors Maurizio Bonafede, Michele Dragoni, and Paolo Gasperini, who, despite being retired, continue to offer invaluable guidance.

Data availability

No data was used for the research described in the article.

References

Acocella, V., 2021. Crustal Deformation, in: Volcano-Tectonic Processes. Springer International Publishing, Cham, pp. 41–78. https://doi.org/10.1007/978-3-030-65968-4_2.

Afanasyev, A.A., 2012. Simulation of the properties of a binary carbon dioxide-water mixture under sub- and supercritical conditions. High Temp. 50, 340–347. https://doi.org/10.1134/S0018151X12030017.

Akita, F., Matsumoto, N., 2004. Hydrological responses induced by the Tokachi-oki earthquake in 2003 at hot spring wells in Hokkaido, Japan. Geophys. Res. Lett. 31, 2004GL020433. https://doi.org/10.1029/2004GL020433.

Albano, M., Barba, S., Solaro, G., Pepe, A., Bignami, C., Moro, M., Saroli, M., Stramondo, S., 2017. Aftershocks, groundwater changes and postseismic ground displacements related to pore pressure gradients: Insights from the 2012 Emilia-Romagna earthquake. JGR Solid Earth 122, 5622–5638. https://doi.org/10.1002/2017JB014009.

Alcolea, A., Meier, P., Vilarrasa, V., Olivella, S., Carrera, J., 2024. Hydromechanical modeling of the hydraulic stimulations in borehole PX2 (Pohang, South Korea). Geothermics 120, 103009. https://doi.org/10.1016/j.geothermics.2024.103009.

Alghamdi, A., Hesse, M.A., Chen, J., Ghattas, O., 2020. Bayesian poroelastic aquifer characterization from InSAR surface deformation data. Part I: maximum a posteriori estimate. Water Resour. Res. 56, e2020WR027391. https://doi.org/10.1029/2020WR027391.

Amann, F., Gischig, V., Evans, K., Doetsch, J., Jalali, R., Valley, B., Krietsch, H., Dutler, N., Villiger, L., Brixel, B., Klepikova, M., Kittilä, A., Madonna, C., Wiemer, S., Saar, M.O., Loew, S., Driesner, T., Maurer, H., Giardini, D., 2018. The seismo-hydromechanical behavior during deep geothermal reservoir stimulations: open questions tackled in a decameter-scale in situ stimulation experiment. Solid Earth 9, 115–137. https://doi.org/10.5194/se-9-115-2018.

Andrés, S., Santillán, D., Mosquera, J.C., Cueto-Felgueroso, L., 2019. Thermo-poroelastic analysis of induced seismicity at the basel enhanced geothermal system. Sustainability 11, 6904. https://doi.org/10.3390/su11246904.

Antonioli, A., Piccinini, D., Chiaraluce, L., Cocco, M., 2005. Fluid flow and seismicity pattern: evidence from the 1997 Umbria-Marche (Central Italy) seismic sequence. Geophys. Res. Lett. 32, 2004GL022256. https://doi.org/10.1029/2004GL022256.

Audet, P., Bostock, M.G., Christensen, N.I., Peacock, S.M., 2009. Seismic evidence for overpressured subducted oceanic crust and megathrust fault sealing. Nature 457, 76–78. https://doi.org/10.1038/nature07650.

Bagdassarov, N., 2021. Fundamentals of Rock Physics, 1st ed. Cambridge University Press. https://doi.org/10.1017/9781108380713.

Battistelli, A., Calore, C., Pruess, K., 1997. The simulator TOUGH2/EWASG for modelling geothermal reservoirs with brines and non-condensible gas. Geothermics 26, 437–464. https://doi.org/10.1016/S0375-6505(97)00007-2.

Beeler, N.M., Simpson, R.W., Hickman, S.H., Lockner, D.A., 2000. Pore fluid pressure, apparent friction, and Coulomb failure. J. Geophys. Res. 105, 25533–25542. https://doi.org/10.1029/2000JB900119.

Bejan, A., 2013. Convection Heat Transfer, Fourth edition. Wiley, Hoboken, New Jersey.

Belardinelli, M.E., Bizzarri, A., Cocco, M., 2003. Earthquake triggering by static and dynamic stress changes. J. Geophys. Res. 108, 2002JB001779. https://doi.org/10.1029/2002JB001779.

Belardinelli, M.E., Bonafede, M., Nespoli, M., 2019. Stress heterogeneities and failure mechanisms induced by temperature and pore-pressure increase in volcanic regions. Earth Planet. Sci. Lett. 525, 115765. https://doi.org/10.1016/j.epsl.2019.115765.

Belardinelli, M.E., Nespoli, M., Bonafede, M., 2022. Stress changes caused by exsolution of magmatic fluids within an axisymmetric inclusion. Geophys. J. Int. 230, 870–892. https://doi.org/10.1093/gji/ggac093.

Belferman, M., Agnon, A., 2024. The impact of lake-level fluctuation on earthquake recurrence interval over historical and prehistorical timescales: the case of the dead sea. In: Assani, A., A. (Eds.), Environmental Sciences. IntechOpen. https://doi.org/10.5772/intechopen.113357.

Benisch, K., Wang, W., Delfs, J.-O., Bauer, S., 2020. The OGS-Eclipse code for simulation of coupled multiphase flow and geomechanical processes in the subsurface. Comput. Geosci. 24, 1315–1331. https://doi.org/10.1007/s10596-020-09951-8.

Biot, M.A., 1941. General theory of three-dimensional consolidation. J. Appl. Phys. 12, 155–164. https://doi.org/10.1063/1.1712886.

Blanco-Martín, L., Jahangir, E., Rinaldi, A.P., Rutqvist, J., 2022. Evaluation of possible reactivation of undetected faults during CO 2 injection. Int. J. Greenh. Gas Contr. 121, 103794. https://doi.org/10.1016/j.ijggc.2022.103794.

Bociu, L., Webster, J.T., 2021. Nonlinear quasi-static poroelasticity. J. Differ. Equ. 296, 242–278. https://doi.org/10.1016/j.jde.2021.05.060.

Bonafede, M., Amoruso, A., Crescentini, L., Gottsmann, J.H., Todesco, M., Trasatti, E., 2022. Source modelling from ground deformation and gravity changes at the Campi Flegrei Caldera, Italy. In: Orsi, G., D'Antonio, M., Civetta, L. (Eds.), Campi Flegrei. Springer, Berlin Heidelberg, Berlin, Heidelberg, pp. 283–309. https://doi.org/10.1007/978-3-642-37060-1_11.

Borgia, A., Oldenburg, C.M., Zhang, R., Pan, L., Daley, T.M., Finsterle, S., Ramakrishnan, T.S., 2017. Simulations of CO2 injection into fractures and faults for improving their geophysical characterization at EGS sites. Geothermics 69, 189–201. https://doi.org/10.1016/j.geothermics.2017.05.002.

Bosl, W.J., Nur, A., 2002. Aftershocks and pore fluid diffusion following the 1992 Landers earthquake. J. Geophys. Res. 107. https://doi.org/10.1029/2001JB000155.

Bossart, P., Bernier, F., Birkholzer, J., Bruggeman, C., Connolly, P., Dewonck, S., Fukaya, M., Herfort, M., Jensen, M., Matray, J.-M., Mayor, J.C., Moeri, A., Oyama, T., Schuster, K., Shigeta, N., Vietor, T., Wieczorek, K., 2017. Mont Terri rock laboratory, 20 years of research: introduction, site characteristics and overview of experiments. Swiss J. Geosci. 110, 3–22. https://doi.org/10.1007/s00015-016-0236-1.

Boussinesq, M.J., 1885. Applications des Potentials, A L'etude De L'equilibre Et Du Mouvment Des Solids Elastiques. Gaythier-Villars, Paris.

Boyet, A., De Simone, S., Ge, S., Vilarrasa, V., 2023. Poroelastic stress relaxation, slip stress transfer and friction weakening controlled post-injection seismicity at the Basel Enhanced Geothermal System. Commun. Earth Environ. 4, 104. https://doi.org/10.1038/s43247-023-00764-y.

Broccardo, M., Mignan, A., Grigoli, F., Karvounis, D., Rinaldi, A.P., Danciu, L., Hofmann, H., Milkereit, C., Dahm, T., Zimmermann, G., Hjörleifsdóttir, V., Wiemer, S., 2019. Induced seismicity risk analysis of the hydraulic stimulation of a geothermal well on Geldinganes, Iceland (preprint). In: Risk Assessment, Mitigation and Adaptation Strategies, Socioeconomic and Management Aspects. https://doi.org/10.5194/nhess-2019-331.

Brodsky, E.E., Kanamori, H., 2001. Elastohydrodynamic lubrication of faults. J. Geophys. Res. 106 (B8), 16357–16374. https://doi.org/10.1029/2001JB000430.

Brodsky, E.E., Roeloffs, E., Woodcock, D., Gall, I., Manga, M., 2003. A mechanism for sustained groundwater pressure changes induced by distant earthquakes. J. Geophys. Res. 108, 2002JB002321. https://doi.org/10.1029/2002JB002321.

Brothers, D., Kilb, D., Luttrell, K., Driscoll, N., Kent, G., 2011. Loading of the San Andreas fault by flood-induced rupture of faults beneath the Salton Sea. Nat. Geosci. 4, 486–492. https://doi.org/10.1038/ngeo1184.

Büyükakpınar, P., Cesca, S., Hainzl, S., Jamalreyhani, M., Heimann, S., Dahm, T., 2021. Reservoir-Triggered Earthquakes around the Atatürk Dam (Southeastern Turkey). Front. Earth Sci. 9, 663385. https://doi.org/10.3389/feart.2021.663385.
Caine, J.S., Evans, J.P., Forster, C.B., 1996. Fault zone architecture and permeability structure. Geol 24, 1025. https://doi.org/10.1130/0091-7613(1996)024<1025:FZAAPS>2.3.CO;2.
Cao, Y., Chen, S., Meir, A.J., 2013. Analysis and numerical approximations of equations of nonlinear poroelasticity. Discr. Contin. Dyn. Syst. Ser. B 18 (2013), 1253–1273.
Cao, W., Shi, J.-Q., Durucan, S., Korre, A., 2021. Evaluation of shear slip stress transfer mechanism for induced microseismicity at in Salah CO2 storage site. Int. J. Greenh. Gas Contr. 107, 103302. https://doi.org/10.1016/j.ijggc.2021.103302.
Cao, W., Durucan, S., Shi, J.-Q., Cai, W., Korre, A., Ratouis, T., 2022. Induced seismicity associated with geothermal fluids re-injection: Poroelastic stressing, thermoelastic stressing, or transient cooling-induced permeability enhancement? Geothermics 102, 102404. https://doi.org/10.1016/j.geothermics.2022.102404.
Cappa, F., Scuderi, M.M., Collettini, C., Guglielmi, Y., Avouac, J.-P., 2019. Stabilization of fault slip by fluid injection in the laboratory and in situ. Sci. Adv. 5, eaau4065. https://doi.org/10.1126/sciadv.aau4065.
Cappa, F., Guglielmi, Y., Nussbaum, C., De Barros, L., Birkholzer, J., 2022. Fluid migration in low-permeability faults driven by decoupling of fault slip and opening. Nat. Geosci. 15, 747–751. https://doi.org/10.1038/s41561-022-00993-4.
Carcione, J.M., Santos, J.E., Picotti, S., 2011. Anisotropic poroelasticity and wave-induced fluid flow: harmonic finite-element simulations: wave-induced fluid flow. Geophys. J. Int. 186, 1245–1254. https://doi.org/10.1111/j.1365-246X.2011.05101.x.
Carminati, E., Martinelli, G., 2002. Subsidence rates in the Po Plain, northern Italy: the relative impact of natural and anthropogenic causation. Eng. Geol. 66, 241–255. https://doi.org/10.1016/S0013-7952(02)00031-5.
Catalli, F., Meier, M., Wiemer, S., 2013. The role of Coulomb stress changes for injection-induced seismicity: the Basel enhanced geothermal system. Geophys. Res. Lett. 40, 72–77. https://doi.org/10.1029/2012GL054147.
Catalli, F., Rinaldi, A.P., Gischig, V., Nespoli, M., Wiemer, S., 2016. The importance of earthquake interactions for injection-induced seismicity: Retrospective modeling of the Basel Enhanced Geothermal System. Geophys. Res. Lett. 43, 4992–4999. https://doi.org/10.1002/2016GL068932.
Cesca, S., Stich, D., Grigoli, F., Vuan, A., López-Comino, J.Á., Niemz, P., Blanch, E., Dahm, T., Ellsworth, W.L., 2021. Seismicity at the Castor gas reservoir driven by pore pressure diffusion and asperities loading. Nat. Commun. 12, 4783. https://doi.org/10.1038/s41467-021-24949-1.
Chang, K.W., Yoon, H., Kim, Y., Lee, M.Y., 2020. Operational and geological controls of coupled poroelastic stressing and pore-pressure accumulation along faults: Induced earthquakes in Pohang, South Korea. Sci. Rep. 10, 2073. https://doi.org/10.1038/s41598-020-58881-z.
Cheng, Y., Liu, W., Xu, T., Zhang, Y., Zhang, X., Xing, Y., Feng, B., Xia, Y., 2023. Seismicity induced by geological CO2 storage: A review. Earth Sci. Rev. 239, 104369. https://doi.org/10.1016/j.earscirev.2023.104369.
Chiarabba, C., Buttinelli, M., Cattaneo, M., De Gori, P., 2020. Large earthquakes driven by fluid overpressure: the apennines normal faulting system case. Tectonics 39, e2019TC006014. https://doi.org/10.1029/2019TC006014.
Chiodini, G., Todesco, M., Caliro, S., Del Gaudio, C., Macedonio, G., Russo, M., 2003. Magma degassing as a trigger of bradyseismic events: the case of Phlegrean Fields (Italy). Geophys. Res. Lett. 30, 2002GL016790. https://doi.org/10.1029/2002GL016790.
Chiodini, G., Caliro, S., Avino, R., Bini, G., Giudicepietro, F., De Cesare, W., Ricciolino, P., Aiuppa, A., Cardellini, C., Petrillo, Z., Selva, J., Siniscalchi, A., Tripaldi, S., 2021. Hydrothermal pressure-temperature control on CO2 emissions and seismicity at Campi Flegrei (Italy). J. Volcanol. Geotherm. Res. 414, 107245. https://doi.org/10.1016/j.jvolgeores.2021.107245.
CMG, 2003. User's Guide STARS. Computer Modelling Group Ltd., Calgary, Canada. https://www.cmgl.ca/stars.
CMG, 2021. GEM Compositional and Unconventional Simulator. https://www.cmgl.ca/gem.
Cocco, M., Rice, J.R., 2002. Pore pressure and poroelasticity effects in Coulomb stress analysis of earthquake interactions. J.-Geophys.-Res. 107. https://doi.org/10.1029/2000JB000138.
Coco, A., Currenti, G., Gottsmann, J., Russo, G., Del Negro, C., 2016. A hydro-geophysical simulator for fluid and mechanical processes in volcanic areas. J.Math. Industry 6, 6. https://doi.org/10.1186/s13362-016-0020-x.
COMSOL, 2012. Comsol Multiphysics 4,3. Comsol Ab, Stockholm. https://www.comsol.it/.
Convertito, V., Catalli, F., Emolo, A., 2013. Combining stress transfer and source directivity: the case of the 2012 Emilia seismic sequence. Sci. Rep. 3, 3114. https://doi.org/10.1038/srep03114.
Currenti, G.M., Napoli, R., 2017. Learning about hydrothermal volcanic activity by modeling induced geophysical changes. Front. Earth Sci. 5, 41. https://doi.org/10.3389/feart.2017.00041.
Currenti, G., Napoli, R., Stissi, S.C., 2024. THEPORE: A software package for modeling THErmo-PORo-elastic displacements. Comput. Geosci. https://doi.org/10.1016/j.cageo.2024.105716.
D'Agostino, N., Silverii, F., Amoroso, O., Convertito, V., Fiorillo, F., Ventafridda, G., Zollo, A., 2018. Crustal deformation and seismicity modulated by groundwater recharge of Karst Aquifers. Geophys. Res. Lett. 45. https://doi.org/10.1029/2018GL079794.
Dal Zilio, L., Gerya, T., 2022. Subduction earthquake cycles controlled by episodic fluid pressure cycling. Lithos 426–427, 106800. https://doi.org/10.1016/j.lithos.2022.106800.
Dal Zilio, L., Lapusta, N., Avouac, J., 2020. unraveling scaling properties of slow-slip events. Geophys. Res. Lett. 47, e2020GL087477. https://doi.org/10.1029/2020GL087477.
Dal Zilio, L., Hegyi, B., Behr, W., Gerya, T., 2022. Hydro-mechanical earthquake cycles in a poro-visco-elasto-plastic fluid-bearing fault structure. Tectonophysics 838, 229516. https://doi.org/10.1016/j.tecto.2022.229516.
Darcy, N., 1856. Les fontaines publiques de la ville de Dijon- Les principes à suivre et les formules à employer dans les distribution d'eau.
De Barros, L., Guglielmi, Y., Rivet, D., Cappa, F., Duboeuf, L., 2018. Seismicity and fault aseismic deformation caused by fluid injection in decametric in-situ experiments. Compt. Rend. Géosci. 350, 464–475. https://doi.org/10.1016/j.crte.2018.08.002.
De Siena, L., Amoruso, A., Petrosino, S., Crescentini, L., 2024. Geophysical responses to an environmentally-boosted volcanic unrest. Geophys. Res. Lett. 51, e2023GL104895. https://doi.org/10.1029/2023GL104895.
Del Gaudio, C., Aquino, I., Ricciardi, G.P., Ricco, C., Scandone, R., 2010. Unrest episodes at Campi Flegrei: A reconstruction of vertical ground movements during 1905–2009. J. Volcanol. Geotherm. Res. 195, 48–56. https://doi.org/10.1016/j.jvolgeores.2010.05.014.
Deng, K., Liu, Y., Harrington, R.M., 2016. Poroelastic stress triggering of the December 2013 Crooked Lake, Alberta, induced seismicity sequence. Geophys. Res. Lett. 43, 8482–8491. https://doi.org/10.1002/2016GL070421.
Deng, F., Dixon, T.H., Xie, S., 2020. Surface deformation and induced seismicity due to fluid injection and oil and gas extraction in Western Texas. JGR Solid Earth 125, e2019JB018962. https://doi.org/10.1029/2019JB018962.
Dieterich, J.H., 2007. Applications of rate- and state-dependent friction to models of fault-slip and earthquake occurrence. In: Treatise on Geophysics. Elsevier, pp. 93–110. https://doi.org/10.1016/B978-0-444-53802-4.00075-0.
Dieterich, J.H., Linker, M.F., 1992. Fault stability under conditions of variable normal stress. Geophys. Res. Lett. 19, 1691–1694. https://doi.org/10.1029/92GL01821.
Durá-Gómez, I., Talwani, P., 2010. Reservoir-induced seismicity associated with the Itoiz Reservoir, Spain: a case study. Geophys. J. Int. 181, 343–356. https://doi.org/10.1111/j.1365-246X.2009.04462.x.
Dutler, N.O., Valley, B., Amann, F., Jalali, M., Villiger, L., Krietsch, H., Gischig, V., Doetsch, J., Giardini, D., 2021. Poroelasticity contributes to hydraulic-stimulation induced pressure changes. Geophys. Res. Lett. 48, e2020GL091468. https://doi.org/10.1029/2020GL091468.
Edmonds, M., Woods, A.W., 2018. Exsolved volatiles in magma reservoirs. J. Volcanol. Geotherm. Res. 368, 13–30. https://doi.org/10.1016/j.jvolgeores.2018.10.018.
Elkhoury, J.E., Brodsky, E.E., Agnew, D.C., 2006. Seismic waves increase permeability. Nature 441, 1135–1138. https://doi.org/10.1038/nature04798.
Ellsworth, W.L., 2013. Injection-induced earthquakes. Science 341, 1225942. https://doi.org/10.1126/science.1225942.
Eshelby, J.D., 1957. The determination of the elastic field of an ellipsoidal inclusion, and related problems. Proc. R. Soc. Lond. A 241, 376–396. https://doi.org/10.1098/rspa.1957.0133.
Evans, J.P., Forster, C.B., Goddard, J.V., 1997. Permeability of fault-related rocks, and implications for hydraulic structure of fault zones. J. Struct. Geol. 19, 1393–1404. https://doi.org/10.1016/S0191-8141(97)00057-6.
Evans, K.F., Zappone, A., Kraft, T., Deichmann, N., Moia, F., 2012. A survey of the induced seismic responses to fluid injection in geothermal and CO2 reservoirs in Europe. Geothermics 41, 30–54. https://doi.org/10.1016/j.geothermics.2011.08.002.
Fan, Z., Eichhubl, P., Newell, P., 2019. Basement fault reactivation by fluid injection into sedimentary reservoirs: poroelastic effects. JGR Solid Earth 124, 7354–7369. https://doi.org/10.1029/2018JB017062.
Flóvenz, Ó.G., Wang, R., Hersir, G.P., Dahm, T., Hainzl, S., Vassileva, M., Drouin, V., Heimann, S., Isken, M.P., Gudnason, E.Á., Ágústsson, K., Ágústsdóttir, T., Horálek, J., Motagh, M., Walter, T.R., Rivalta, E., Jousset, P., Krawczyk, C.M., Milkereit, C., 2022. Cyclical geothermal unrest as a precursor to Iceland's 2021 Fagradalsfjall eruption. Nat. Geosci. 15, 397–404. https://doi.org/10.1038/s41561-022-00930-5.
Fournier, N., Chardot, L., 2012. Understanding volcano hydrothermal unrest from geodetic observations: Insights from numerical modeling and application to White Island volcano, New Zealand. J. Geophys. Res. 117, 2012JB009469. https://doi.org/10.1029/2012JB009469.
Freed, A.M., Bürgmann, R., Calais, E., Freymueller, J., Hreinsdóttir, S., 2006. Implications of deformation following the 2002 Denali, Alaska, earthquake for postseismic relaxation processes and lithospheric rheology. J. Geophys. Res. 111, 2005JB003894. https://doi.org/10.1029/2005JB003894.
Fung, Y., 1965. Foundations of Solid Mechanics. In: Prentice Hall international series in dynamics. Prentice-Hall, Englewood Cliffs (N.J.).
Fyfe, W.S., 1978. Fluids in the Earth's Crust: Their Significance in Metamorphic, Tectonic And Chemical Transport Process. Elsevier Science, Amsterdam.
Gao, X., Wang, K., 2017. Rheological separation of the megathrust seismogenic zone and episodic tremor and slip. Nature 543, 416–419. https://doi.org/10.1038/nature21389.
Ge, S., Saar, M.O., 2022. Review: induced seismicity during geoenergy development—a hydromechanical perspective. JGR Solid Earth 127, e2021JB023141. https://doi.org/10.1029/2021JB023141.
Ge, S., Stover, S.C., 2000. Hydrodynamic response to strike- and dip-slip faulting in a half-space. J. Geophys. Res. 105, 25513–25524. https://doi.org/10.1029/2000JB900233.
Ge, S., Liu, M., Lu, N., Godt, J.W., Luo, G., 2009. Did the Zipingpu Reservoir trigger the 2008 Wenchuan earthquake? Geophys. Res. Lett. 36, 2009GL040349. https://doi.org/10.1029/2009GL040349.
Geballe, Z.M., Wang, C.-Y., Manga, M., 2011. A permeability-change model for water-level changes triggered by teleseismic waves: A permeability-change model for water

level changes. Geofluids 11, 302–308. https://doi.org/10.1111/j.1468-8123.2011.00341.x.
Geertsma, J., 1966. Problems of Rock Mechanics in Petroleum Production Engineering. N. p, Portugal.
Geertsma, J., 1973. Land subsidence above compacting oil and gas reservoirs. J. Pet. Technol. 25, 734–744. https://doi.org/10.2118/3730-PA.
Gischig, V.S., Wiemer, S., 2013. A stochastic model for induced seismicity based on non-linear pressure diffusion and irreversible permeability enhancement. Geophys. J. Int. 194, 1229–1249. https://doi.org/10.1093/gji/ggt164.
Goetze, C., Evans, B., 1979. Stress and temperature in the bending lithosphere as constrained by experimental rock mechanics. Geophys. J. Int. 59, 463–478. https://doi.org/10.1111/j.1365-246X.1979.tb02567.x.
Gottsmann, J., Komorowski, J.-C., Barclay, J., 2017. Volcanic unrest and pre-eruptive processes: a hazard and risk perspective. In: Gottsmann, Joachim, Neuberg, J., Scheu, B. (Eds.), Volcanic Unrest, Advances in Volcanology. Springer International Publishing, Cham, pp. 1–21. https://doi.org/10.1007/11157_2017_19.
Gratier, J.-P., Dysthe, D.K., Renard, F., 2013. The role of pressure solution creep in the ductility of the Earth's upper crust. In: Advances in Geophysics. Elsevier, pp. 47–179. https://doi.org/10.1016/B978-0-12-380940-7.00002-0.
Grigoli, F., Cesca, S., Priolo, E., Rinaldi, A.P., Clinton, J.F., Stabile, T.A., Dost, B., Fernandez, M.G., Wiemer, S., Dahm, T., 2017. Current challenges in monitoring, discrimination, and management of induced seismicity related to underground industrial activities: A European perspective. Rev. Geophys. 55, 310–340. https://doi.org/10.1002/2016RG000542.
Grünthal, G., 2014. Induced seismicity related to geothermal projects versus natural tectonic earthquakes and other types of induced seismic events in Central Europe. Geothermics 52, 22–35. https://doi.org/10.1016/j.geothermics.2013.09.009.
Guglielmi, Y., Cappa, F., Avouac, J.-P., Henry, P., Elsworth, D., 2015. Seismicity triggered by fluid injection–induced aseismic slip. Science 348, 1224–1226. https://doi.org/10.1126/science.aab0476.
Guglielmi, Y., Nussbaum, C., Cappa, F., De Barros, L., Rutqvist, J., Birkholzer, J., 2021. Field-scale fault reactivation experiments by fluid injection highlight aseismic leakage in caprock analogs: Implications for CO2 sequestration. Int. J. Greenh. Gas Contr. 111, 103471. https://doi.org/10.1016/j.ijggc.2021.103471.
Guido, F.L., Antonellini, M., Picotti, V., 2015. Modeling ground displacement above reservoirs undergoing fluid withdrawal/injection based on an ellipsoidal inhomogeneity model. Int. J. Rock Mech. Min. Sci. 79, 63–69. https://doi.org/10.1016/j.ijrmms.2015.08.010.
Gupta, H.K., 2002. A review of recent studies of triggered earthquakes by artificial water reservoirs with special emphasis on earthquakes in Koyna, India. Earth Sci. Rev. 58, 279–310. https://doi.org/10.1016/S0012-8252(02)00063-6.
Hainzl, S., Ogata, Y., 2005. Detecting fluid signals in seismicity data through statistical earthquake modeling. J. Geophys. Res. 110, 2004JB003247. https://doi.org/10.1029/2004JB003247.
Harbaugh, A.W., 2005. Techniques and Methods (Techniques and Methods).
Häring, M.O., Schanz, U., Ladner, F., Dyer, B.C., 2008. Characterisation of the Basel 1 enhanced geothermal system. Geothermics 37, 469–495. https://doi.org/10.1016/j.geothermics.2008.06.002.
Harris, R.A., 1998. Introduction to special section: stress triggers, stress shadows, and implications for seismic hazard. J. Geophys. Res. 103, 24347–24358. https://doi.org/10.1029/98JB01576.
Harris, R.A., Day, S.M., 1999. Dynamic 3D simulations of earthquakes on En Echelon Faults. Geophys. Res. Lett. 26, 2089–2092. https://doi.org/10.1029/1999GL900377.
Heimisson, E.R., Dunham, E.M., Almquist, M., 2019. Poroelastic effects destabilize mildly rate-strengthening friction to generate stable slow slip pulses. J. Mech. Phys. Solids 130, 262–279. https://doi.org/10.1016/j.jmps.2019.06.007.
Hill, R.G., Weingarten, M., Rockwell, T.K., Fialko, Y., 2023. Major southern San Andreas earthquakes modulated by lake-filling events. Nature 618, 761–766. https://doi.org/10.1038/s41586-023-06058-9.
Holzer, T.L., 1984. Man-Induced Land Subsidence, Reviews in Engineering Geology. Geological Society of America. https://doi.org/10.1130/REG6.
Hopp, C., Guglielmi, Y., Rinaldi, A.P., Soom, F., Wenning, Q., Cook, P., Robertson, M., Kakurina, M., Zappone, A., 2022. The effect of fault architecture on slip behavior in shale revealed by distributed fiber optic strain sensing. JGR Solid Earth 127, e2021JB022432. https://doi.org/10.1029/2021JB022432.
Hough, S.E., Tsai, V.C., Walker, R., Aminzadeh, F., 2017. Was the Mw 7.5 1952 Kern County, California, earthquake induced (or triggered)? J. Seismol. 21, 1613–1621. https://doi.org/10.1007/s10950-017-9685-x.
Hsieh, P.A., 1996. Deformation-induced changes in hydraulic head during ground-water withdrawal. Groundwater 34, 1082–1089. https://doi.org/10.1111/j.1745-6584.1996.tb02174.x.
Hsieh, P.A., Ingebritsen, S.E., 2019. Groundwater inflow toward a preheated volcanic conduit: application to the 2018 Eruption at Kīlauea Volcano, Hawai'i. JGR Solid Earth 124, 1498–1506. https://doi.org/10.1029/2018JB017133.
Hua, W., Chen, Z., Zheng, S., Yan, C., 2013. Reservoir-induced seismicity in the Longtan reservoir, southwestern China. J. Seismol. 17, 667–681. https://doi.org/10.1007/s10950-012-9345-0.
Huang, F., Li, M., Ma, Y., Han, Y., Tian, L., Yan, W., Li, X., 2017. Studies on earthquake precursors in China: A review for recent 50 years. Geodesy. Geodyn. 8, 1–12. https://doi.org/10.1016/j.geog.2016.12.002.
Hughes, K.L.H., Masterlark, T., Mooney, W.D., 2010. Poroelastic stress-triggering of the 2005 M8.7 Nias earthquake by the 2004 M9.2 Sumatra–Andaman earthquake. Earth Planet. Sci. Lett. 293, 289–299. https://doi.org/10.1016/j.epsl.2010.02.043.
Hurwitz, S., Christiansen, L.B., Hsieh, P.A., 2007. Hydrothermal fluid flow and deformation in large calderas: Inferences from numerical simulations. J. Geophys. Res. 112, 2006JB004689. https://doi.org/10.1029/2006JB004689.
Ikari, M.J., Marone, C., Saffer, D.M., Kopf, A.J., 2013. Slip weakening as a mechanism for slow earthquakes. Nat. Geosci. 6, 468–472. https://doi.org/10.1038/ngeo1818.
Ikeuchi, K., Doi, N., Sakagawa, Y., Kamenosono, H., Uchida, T., 1998. High-temperature measurements in well WD-1A and the thermal structure of the kakkonda geothermal system, Japan. Geothermics 27, 591–607. https://doi.org/10.1016/S0375-6505(98)00035-2.
Ingebritsen, S.E., Manning, C.E., 2010. Permeability of the continental crust: dynamic variations inferred from seismicity and metamorphism. Geofluids 10, 193–205. https://doi.org/10.1111/j.1468-8123.2010.00278.x.
Ingebritsen, S.E., Sanford, W.E., Neuzil, C.E., 2006. Groundwater in Geologic Processes, 2nd ed. Cambridge University Press, Cambridge, New York.
Itaba, S., Koizumi, N., Matsumoto, N., Ohtani, R., 2010. Continuous observation of groundwater and crustal deformation for forecasting Tonankai and Nankai Earthquakes in Japan. Pure Appl. Geophys. 167, 1105–1114. https://doi.org/10.1007/s00024-010-0095-z.
Itasca, 2009. FLAC3D, Fast Lagrangian Analysis of Continua in 3 Dimensions, Version 4.0. Itasca Consulting Group, Minneapolis, Minnesota, 438pp.
Jeanne, P., Rutqvist, J., Rinaldi, A.P., Dobson, P.F., Walters, M., Hartline, C., Garcia, J., 2015. Seismic and aseismic deformations and impact on reservoir permeability: the case of EGS stimulation at the Geysers, California, USA. JGR Solid Earth 120, 7863–7882. https://doi.org/10.1002/2015JB012142.
Jin, L., 2022. A hydromechanical-stochastic approach to modeling fluid-induced seismicity in arbitrarily fractured poroelastic media: Effects of fractures and coupling. Tectonophysics 826, 229249. https://doi.org/10.1016/j.tecto.2022.229249.
Johri, M., Zoback, M.D., Hennings, P., 2014. A scaling law to characterize fault-damage zones at reservoir depths. Bulletin 98, 2057–2079. https://doi.org/10.1306/05061413173.
Jónsson, S., Segall, P., Pedersen, R., Björnsson, G., 2003. Post-earthquake ground movements correlated to pore-pressure transients. Nature 424, 179–183. https://doi.org/10.1038/nature01776.
Jung, Y., Pau, G.S.H., Finsterle, S., Pollyea, R.M., 2017. TOUGH3: A new efficient version of the TOUGH suite of multiphase flow and transport simulators. Comput. Geosci. 108, 2–7. https://doi.org/10.1016/j.cageo.2016.09.009.
Karato, S., Karki, B., Park, J., 2020. Deep mantle melting, global water circulation and its implications for the stability of the ocean mass. Prog. Earth Planet. Sci. 7, 76. https://doi.org/10.1186/s40645-020-00379-3.
Karegar, M.A., Dixon, T.H., Malservisi, R., Yang, Q., Hossaini, S.A., Hovorka, S.D., 2015. GPS-based monitoring of surface deformation associated with CO2 injection at an enhanced oil recovery site. Int. J. Greenh. Gas Contr. 41, 116–126. https://doi.org/10.1016/j.ijggc.2015.07.006.
Kariche, J., Meghraoui, M., 2021. Stress transfer and poroelasticity associated to major earthquakes in Africa. Arab. J. Geosci. 14, 787. https://doi.org/10.1007/s12517-021-07132-0.
Kariche, J., Meghraoui, M., Timoulali, Y., Cetin, E., Toussaint, R., 2018. The Al Hoceima earthquake sequence of 1994, 2004 and 2016: stress transfer and poroelasticity in the Rif and Alboran Sea region. Geophys. J. Int. 212, 42–53. https://doi.org/10.1093/gji/ggx385.
Keranen, K.M., Weingarten, M., Abers, G.A., Bekins, B.A., Ge, S., 2014. Sharp increase in Central Oklahoma seismicity since 2008 induced by massive wastewater injection. Science 345, 448–451. https://doi.org/10.1126/science.1255802.
Khan, C., Amin, R., Madden, G., 2013. Carbon dioxide injection for enhanced gas recovery and storage (reservoir simulation). Egypt. J. Pet. 22, 225–240. https://doi.org/10.1016/j.ejpe.2013.06.002.
Kim, Y.-S., Peacock, D.C.P., Sanderson, D.J., 2004. Fault damage zones. J. Struct. Geol. 26, 503–517. https://doi.org/10.1016/j.jsg.2003.08.002.
King, G.C.P., Stein, R.S., Lin, L., 1994. Static stress changes and the triggering of earthquakes. Bull. Seismol. Soc. Am. 84 (3), 935–953. https://doi.org/10.1785/BSSA0840030935.
Kipp, K.L., Hsieh, P.A., Charlton, 2008. Guide to the revised ground-water flow and heat transport simulator: HYDROTHERM — Version 3: U.S. Geol. Surv. Tech. Methods 6–A25, 160 p.
Kneafsey, T.J., Dobson, P.F., Ulrich, C., Hopp, C., Rodríguez-Tribaldos, V., Guglielmi, Y., Blankenship, D., Schwering, P.C., Ingraham, M., Burghardt, J.A., White, M.D., Johnson, T.C., Strickland, C., Vermuel, V., Knox, H.A., Morris, J.P., Fu, P., Smith, M., Wu, H., Ajo-Franklin, J.B., Huang, L., Neupane, G., Horne, R., Roggenthen, W., Weers, J., Doe, T.W., Pyatina, T., Team, E.C., 2022. The EGS collab project – stimulations at two depths. In: All Days. Presented at the 56th U.S. Rock Mechanics/Geomechanics Symposium. ARMA, Santa Fe, New Mexico, USA. https://doi.org/10.56952/ARMA-2022-2261 p. ARMA-2022-2261.
Koutsabeloulis, N.C., Hope, S.A., 1998. "Coupled" Stress/fluid/thermal multi-phase reservoir simulation studies incorporating rock mechanics. In: All Days. Presented at the SPE/ISRM Rock Mechanics in Petroleum Engineering. SPE, Trondheim, Norway. https://doi.org/10.2118/47393-MS p. SPE-47393-MS.
Kümpel, H.-J., 1991. Poroelasticity: parameters reviewed. Geophys. J. Int. 105, 783–799. https://doi.org/10.1111/j.1365-246X.1991.tb00813.x.
Kümpel, H.-J., 1992. About the potential of wells to reflect stress variations within inhomogeneous crust. Tectonophysics 211, 317–336. https://doi.org/10.1016/0040-1951(92)90068-H.
Kutsienyo, E.J., Appold, M.S., White, M.D., Ampomah, W., 2021. Numerical modeling of CO2 sequestration within a five-spot well pattern in the Morrow B sandstone of the farnsworth hydrocarbon field: comparison of the TOUGHREACT, STOMP-EOR, and GEM simulators. Energies 14, 5337. https://doi.org/10.3390/en14175337.

Lai, G., Lei, X., Jiang, C., Wang, W., Gong, H., 2021. Multiple mechanisms of coseismic water level changes at the Rongchang well in a seismically active area in China. Tectonophysics 819, 229083. https://doi.org/10.1016/j.tecto.2021.229083.
Liu, Y., Rubin, A.M., 2010. Role of fault gouge dilatancy on aseismic deformation transients. J. Geophys. Res. 115, 2010JB007522. https://doi.org/10.1029/2010JB007522.
Liu, F., Wang, G., Zhang, W., Yue, C., Tao, L., 2020. Using TOUGH2 numerical simulation to analyse the geothermal formation in Guide basin, China. J. Groundw. Sci. Eng. 8 (4), 328–337. https://doi.org/10.19637/j.cnki.2305-7068.2020.04.003.
Liu, C.-Y., Chia, Y., Chung, P.-Y., Lee, T.-P., Chiu, Y.-C., 2023. Temporal variation and spatial distribution of groundwater level changes induced by large earthquakes. Water 15, 357. https://doi.org/10.3390/w15020357.
Ma, X., Hertrich, M., Amann, F., Bröker, K., Gholizadeh Doonechaly, N., Gischig, V., Hochreutener, R., Kästli, P., Krietsch, H., Marti, M., Nägeli, B., Nejati, M., Obermann, A., Plenkers, K., Rinaldi, A.P., Shakas, A., Villiger, L., Wenning, Q., Zappone, A., Bethmann, F., Castilla, R., Seberto, F., Meier, P., Driesner, T., Loew, S., Maurer, H., Saar, M.O., Wiemer, S., Giardini, D., 2022. Multi-disciplinary characterizations of the BedrettoLab – a new underground geoscience research facility. Solid Earth 13, 301–322. https://doi.org/10.5194/se-13-301-2022.
Malagnini, L., Parsons, T., Munafò, I., Mancini, S., Segou, M., Geist, E.L., 2022. Crustal permeability changes inferred from seismic attenuation: Impacts on multi-mainshock sequences. Front. Earth Sci. 10, 963689. https://doi.org/10.3389/feart.2022.963689.
Mandal, P., Kumar, M., Biswas, K., 2016. Evidence for a fluid flow triggered spatio-temporal migration of seismicity in the 2001 Mw 7.7 Bhuj earthquake region, Gujarat, India, during 2001–2013. J. Earth Syst. Sci. 125, 1285–1298. https://doi.org/10.1007/s12040-016-0729-3.
Mandler, E., Pintori, F., Gualandi, A., Anderlini, L., Serpelloni, E., Belardinelli, M.E., 2021. Post-seismic deformation related to the 2016 Central Italy seismic sequence from GPS displacement time-series. JGR Solid Earth 126, e2021JB022200. https://doi.org/10.1029/2021JB022200.
Mandler, E., Canitano, A., Belardinelli, M.E., Nespoli, M., Serpelloni, E., Linde, A., 2024. Tidal calibration of the gladwin tensor strain monitor (GTSM) array in Taiwan. Pure Appl. Geophys. https://doi.org/10.1007/s00024-024-03453-9.
Manga, M., Wang, C.-Y., 2015. Earthquake hydrology. In: Treatise on Geophysics. Elsevier, pp. 305–328. https://doi.org/10.1016/B978-0-444-53802-4.00082-8.
Manga, M., Beresnev, I., Brodsky, E.E., Elkhoury, J.E., Elsworth, D., Ingebritsen, S.E., Mays, D.C., Wang, C., 2012. Changes in permeability caused by transient stresses: Field observations, experiments, and mechanisms. Rev. Geophys. 50, 2011RG000382. https://doi.org/10.1029/2011RG000382.
Mannen, K., Roman, D., Leonard, G., Prejean, S., Nakagawa, M., 2019. Special issue "Towards forecasting phreatic eruptions: examples from Hakone volcano and some global equivalents". Earth Planets Space 71, 91. https://doi.org/10.1186/s40623-019-1068-9.
Mantiloni, L., Nespoli, M., Belardinelli, M.E., Bonafede, M., 2020. Deformation and stress in hydrothermal regions: the case of a disk-shaped inclusion in a half-space. J. Volcanol. Geotherm. Res. 403, 107011. https://doi.org/10.1016/j.jvolgeores.2020.107011.
Marema, T.M., Molwalefhe, L., Shemang, E.M., 2023. Characterisation of the hydrogeological properties of the Ntane Sandstone aquifer using Co-seismic and post-seismic groundwater level responses to the Mw 6.5 Moiyabana Earthquake, Central Botswana. Water 15, 1947. https://doi.org/10.3390/w15101947.
Markov, M., Markov, A., Levin, V., Sabina, F.J., 2022. Electromagnetic field generated by acoustic wave scattering at a poroelastic inclusion located in a fluid. Int. J. Eng. Sci. 181, 103766. https://doi.org/10.1016/j.ijengsci.2022.103766.
Markovich, K.H., Manning, A.H., Condon, L.E., McIntosh, J.C., 2019. Mountain-block recharge: a review of current understanding. Water Resour. Res. 55, 8278–8304. https://doi.org/10.1029/2019WR025676.
Marone, C., 1998. Laboratory-derived friction laws and their application to seismic faulting. Annu. Rev. Earth Planet. Sci. 26, 643–696. https://doi.org/10.1146/annurev.earth.26.1.643.
McCormack, K., Hesse, M.A., Dixon, T., Malservisi, R., 2020. Modeling the contribution of poroelastic deformation to postseismic geodetic signals. Geophys. Res. Lett. 47, e2020GL086945. https://doi.org/10.1029/2020GL086945.
McTigue, D.F., 1986. Thermoelastic response of fluid-saturated porous rock. J. Geophys. Res. 91, 9533–9542. https://doi.org/10.1029/JB091iB09p09533.
Mehmani, Y., Balhoff, M.T., 2015. Mesoscale and hybrid models of fluid flow and solute transport. Rev. Mineral. Geochem. 80, 433–459. https://doi.org/10.2138/rmg.2015.80.13.
Mignan, A., Broccardo, M., Wiemer, S., Giardini, D., 2017. Induced seismicity closed-form traffic light system for actuarial decision-making during deep fluid injections. Sci. Rep. 7, 13607. https://doi.org/10.1038/s41598-017-13585-9.
Miller, S.A., 2013. The role of fluids in tectonic and earthquake processes. In: Advances in Geophysics. Elsevier, pp. 1–46. https://doi.org/10.1016/B978-0-12-380940-7.00001-9.
Miller, S.A., Collettini, C., Chiaraluce, L., Cocco, M., Barchi, M., Kaus, B.J.P., 2004. Aftershocks driven by a high-pressure CO2 source at depth. Nature 427, 724–727. https://doi.org/10.1038/nature02251.
Minarelli, L., Amoroso, S., Civico, R., De Martini, P.M., Lugli, S., Martelli, L., Molisso, F., Rollins, K.M., Salocchi, A., Stefani, M., Cultrera, G., Milana, G., Fontana, D., 2022. Liquefied sites of the 2012 Emilia earthquake: a comprehensive database of the geological and geotechnical features (Quaternary alluvial Po plain, Italy). Bull. Earthq. Eng. 20, 3659–3697. https://doi.org/10.1007/s10518-022-01338-7.
Mitsui, Y., Cocco, M., 2010. The Role of porosity evolution and fluid flow in frictional instabilities: a parametric study using a spring-slider dynamic system. Geophys. Res. Lett. 37, L23305. https://doi.org/10.1029/2010GL045672.
Moein, M.J.A., Langenbruch, C., Schultz, R., Grigoli, F., Ellsworth, W.L., Wang, R., Rinaldi, A.P., Shapiro, S., 2023. The physical mechanisms of induced earthquakes. Nat. Rev. Earth Environ. 4, 847–863. https://doi.org/10.1038/s43017-023-00497-8.
Mogi, K., 1958. Relations between the Eruptions of various Volcanoes and the Deformations of the Ground Surfaces around them. Bull. Earthq. Res. Inst. 36, 99–134.
MSC, 2015. MSC Software Corporation. Marc. Volume A: Theory and User Information.
NAGRA, 2016. Technical Report 14–13: High-Level Waste Respository-Induced Effects.
Narita, S., Ozawa, T., Aoki, Y., Shimada, M., Furuya, M., Takada, Y., Murakami, M., 2020. Precursory ground deformation of the 2018 phreatic eruption on Iwo-Yama volcano, revealed by four-dimensional joint analysis of airborne and spaceborne InSAR. Earth Planets Space 72, 145. https://doi.org/10.1186/s40623-020-01280-5.
National Research Council, 2013. Induced Seismicity Potential in Energy Technologies. National Academies Press, Washington, D.C.. https://doi.org/10.17226/13355
Nespoli, M., Todesco, M., Serpelloni, E., Belardinelli, M.E., Bonafede, M., Marcaccio, M., Rinaldi, A.P., Anderlini, L., Gualandi, A., 2016. Modeling earthquake effects on groundwater levels: evidences from the 2012 Emilia earthquake (Italy). Geofluids 16, 452–463. https://doi.org/10.1111/gfl.12165.
Nespoli, M., Belardinelli, M.E., Anderlini, L., Bonafede, M., Pezzo, G., Todesco, M., Rinaldi, A.P., 2017. Effects of layered crust on the coseismic slip inversion and related CFF variations: Hints from the 2012 Emilia Romagna earthquake. Phys. Earth Planet. Inter. 273, 23–35. https://doi.org/10.1016/j.pepi.2017.10.011.
Nespoli, M., Belardinelli, M.E., Gualandi, A., Serpelloni, E., Bonafede, M., 2018. Poroelasticity and fluid flow modeling for the 2012 Emilia-Romagna Earthquakes: Hints from GPS and InSAR Data. Geofluids 2018, 1–15. https://doi.org/10.1155/2018/4160570.
Nespoli, M., Belardinelli, M.E., Bonafede, M., 2021a. Stress and deformation induced in layered media by cylindrical thermo-poro-elastic sources: an application to Campi Flegrei (Italy). J. Volcanol. Geotherm. Res. 415, 107269. https://doi.org/10.1016/j.jvolgeores.2021.107269.
Nespoli, M., Cenni, N., Belardinelli, M.E., Marcaccio, M., 2021b. The interaction between displacements and water level changes due to natural and anthropogenic effects in the Po Plain (Italy): the different point of view of GNSS and piezometers. J. Hydrol. 596, 126112. https://doi.org/10.1016/j.jhydrol.2021.126112.
Nespoli, M., Belardinelli, M.E., Calò, M., Tramelli, A., Bonafede, M., 2022. Deformation induced by distributions of single forces in a layered half-space: E F G R N / E F C M P. Comput. Geosci. 164, 105136. https://doi.org/10.1016/j.cageo.2022.105136.
Nespoli, M., Belardinelli, M.E., Bonafede, M., 2023a. Thermo-poro-viscoelastic response of a disc-shaped inclusion. Geophys. J. Int. 235, 135–149. https://doi.org/10.1093/gji/ggad212.
Nespoli, M., Tramelli, A., Belardinelli, M.E., Bonafede, M., 2023b. The effects of hot and pressurized fluid flow across a brittle layer on the recent seismicity and deformation in the Campi Flegrei caldera (Italy). J. Volcanol. Geotherm. Res. 443, 107930. https://doi.org/10.1016/j.jvolgeores.2023.107930.
Nguyen, T.S., 2018. Thermo-hydro-mechanical-chemical processes in geological disposal of radioactive waste – an example of regulatory research. Adv. Geo-Energy Res. 2, 173–189. https://doi.org/10.26804/ager.2018.02.06.
Noda, H., Lapusta, N., 2013. Stable creeping fault segments can become destructive as a result of dynamic weakening. Nature 493, 518–521. https://doi.org/10.1038/nature11703.
Nostro, C., Cocco, M., Belardinelli, M.E., 1997. Static stress changes in extensional regimes: an application to southern Apennines (Italy). Bull. Seismol. Soc. Am. 87, 234–248. https://doi.org/10.1785/BSSA0870010234.
Nostro, C., Chiaraluce, L., Cocco, M., Baumont, D., Scotti, O., 2005. Coulomb stress changes caused by repeated normal faulting earthquakes during the 1997 Umbria-Marche (Central Italy) seismic sequence. J. Geophys. Res. 110, 2004JB003386. https://doi.org/10.1029/2004JB003386.
Nur, A., Booker, J.R., 1972. Aftershocks caused by pore fluid flow? Science 175, 885–887. https://doi.org/10.1126/science.175.4024.885.
Okada, Y., 1992. Internal deformation due to shear and tensile faults in a half-space. Bull. Seismol. Soc. Am. 82, 1018–1040. https://doi.org/10.1785/BSSA0820021018.
Olasolo, P., Juárez, M.C., Morales, M.P., D'Amico, S., Liarte, I.A., 2016. Enhanced geothermal systems (EGS): A review. Renew. Sust. Energ. Rev. 56, 133–144. https://doi.org/10.1016/j.rser.2015.11.031.
Oliveira, B., Afonso, J.C., Zlotnik, S., Diez, P., 2018. Numerical modelling of multiphase multicomponent reactive transport in the Earth's interior. Geophys. J. Int. 212, 345–388. https://doi.org/10.1093/gji/ggx399.
Parotidis, M., Rothert, E., Shapiro, S.A., 2003. Pore-pressure diffusion: A possible triggering mechanism for the earthquake swarms 2000 in Vogtland/NW-Bohemia, Central Europe. Geophys. Res. Lett. 30, 2003GL018110. https://doi.org/10.1029/2003GL018110.
Peikert, J., Hampel, A., Bagge, M., 2022. Relative importance of poroelastic effects and viscoelastic relaxation for postseismic velocity fields after normal and thrust earthquakes: Insights from 2D finite-element modelling. Tectonophysics 838, 229477. https://doi.org/10.1016/j.tecto.2022.229477.
Peltzer, G., Rosen, P., Rogez, F., Hudnut, K., 1998. Poroelastic rebound along the Landers 1992 earthquake surface rupture. J. Geophys. Res. 103, 30131–30145. https://doi.org/10.1029/98JB02302.
Peña, C., Metzger, S., Heidbach, O., Bedford, J., Bookhagen, B., Moreno, M., Oncken, O., Cotton, F., 2022. Role of poroelasticity during the early postseismic deformation of the 2010 Maule Megathrust Earthquake. Geophys. Res. Lett. 49, e2022GL098144. https://doi.org/10.1029/2022GL098144.
Pintori, F., Serpelloni, E., Longuevergne, L., Garcia, A., Faenza, L., D'Alberto, L., Gualandi, A., Belardinelli, M.E., 2021. Mechanical response of shallow crust to groundwater storage variations: inferences from deformation and seismic

observations in the Eastern Southern Alps, Italy. JGR Solid Earth 126, e2020JB020586. https://doi.org/10.1029/2020JB020586.
Piombo, A., Martinelli, G., Dragoni, M., 2005. Post-seismic fluid flow and Coulomb stress changes in a poroelastic medium. Geophys. J. Int. 162, 507–515. https://doi.org/10.1111/j.1365-246X.2005.02673.x.
Prévost, J.H., 1982. Nonlinear transient phenomena in saturated porous media. Comput. Methods Appl. Mech. Eng. 30, 3–18. https://doi.org/10.1016/0045-7825(82)90052-4.
Pruess, K., Oldenburg, C., Moridis, G., 2012. TOUGH2 User's Guide, Version 2.1, Paper LBNL-43134 (Revised). Lawrence Berkeley National Laboratory, Berkeley, CA, USA.
Reynolds, H.I., Gudmundsson, M.T., Högnadóttir, T., Magnússon, E., Pálsson, F., 2017. Subglacial volcanic activity above a lateral dyke path during the 2014–2015 Bárdarbunga-Holuhraun rifting episode, Iceland. Bull. Volcanol. 79, 38. https://doi.org/10.1007/s00445-017-1122-z.
Rice, J.R., 2006. Heating and weakening of faults during earthquake slip. J. Geophys. Res. 111, 2005JB004006. https://doi.org/10.1029/2005JB004006.
Rice, J.R., Cleary, M.P., 1976. Some basic stress diffusion solutions for fluid-saturated elastic porous media with compressible constituents. Rev. Geophys. 14, 227–241. https://doi.org/10.1029/RG014i002p00227.
Rinaldi, A.P., Nespoli, M., 2017. TOUGH2-seed: A coupled fluid flow and mechanical-stochastic approach to model injection-induced seismicity. Comput. Geosci. 108, 86–97. https://doi.org/10.1016/j.cageo.2016.12.003.
Rinaldi, A.P., Rutqvist, J., 2013. Modeling of deep fracture zone opening and transient ground surface uplift at KB-502 CO2 injection well, in Salah, Algeria. Int. J. Greenh. Gas Contr. 12, 155–167. https://doi.org/10.1016/j.ijggc.2012.10.017.
Rinaldi, A.P., Rutqvist, J., 2019. Joint opening or hydroshearing? Analyzing a fracture zone stimulation at Fenton Hill. Geothermics 77, 83–98. https://doi.org/10.1016/j.geothermics.2018.08.006.
Rinaldi, A.P., Todesco, M., Bonafede, M., 2010. Hydrothermal instability and ground displacement at the Campi Flegrei caldera. Phys. Earth Planet. Inter. 178, 155–161. https://doi.org/10.1016/j.pepi.2009.09.005.
Rinaldi, A.P., Rutqvist, J., Cappa, F., 2014. Geomechanical effects on CO2 leakage through fault zones during large-scale underground injection. Int. J. Greenh. Gas Contr. 20, 117–131. https://doi.org/10.1016/j.ijggc.2013.11.001.
Rinaldi, A.P., Rutqvist, J., Sonnenthal, E.L., Cladouhos, T.T., 2015. Coupled THM modeling of hydroshearing stimulation in tight fractured volcanic rock. Transp. Porous Media 108, 131–150. https://doi.org/10.1007/s11242-014-0296-5.
Rinaldi, A.P., Rutqvist, J., Finsterle, S., Liu, H.-H., 2017. Inverse modeling of ground surface uplift and pressure with iTOUGH-PEST and TOUGH-FLAC: the case of CO2 injection at in Salah, Algeria. Comput. Geosci. 108, 98–109. https://doi.org/10.1016/j.cageo.2016.10.009.
Rinaldi, A.P., Improta, L., Hainzl, S., Cataldi, F., Urpi, L., Wiemer, S., 2020. Combined approach of poroelastic and earthquake nucleation applied to the reservoir-induced seismic activity in the Val d'Agri area, Italy. J. Rock Mech. Geotech. Eng. 12, 802–810. https://doi.org/10.1016/j.jrmge.2020.04.003.
Ritz, V.A., Rinaldi, A.P., Zbinden, D., Nespoli, M., Karvounis, D., Wiemer, S., 2020. Modelling induced seismicity with a hydraulic-mechanical-stochastic simulator: review of case studies. In: Presented at the 54th U.S. Rock Mechanics/Geomechanics Symposium p. ARMA-2020-1654.
Ritz, V.A., Rinaldi, A.P., Wiemer, S., 2022. Transient evolution of the relative size distribution of earthquakes as a risk indicator for induced seismicity. Commun. Earth Environ. 3, 249. https://doi.org/10.1038/s43247-022-00581-9.
Roeloffs, E.A., 1988. Fault stability changes induced beneath a reservoir with cyclic variations in water level. J. Geophys. Res. 93, 2107–2124. https://doi.org/10.1029/JB093iB03p02107.
Roeloffs, E., 1996. Poroelastic techniques in the study of earthquake-related hydrologic phenomena. In: Advances in Geophysics. Elsevier, pp. 135–195. https://doi.org/10.1016/S0065-2687(08)60270-8.
Roeloffs, E.A., 1998. Persistent water level changes in a well near Parkfield, California, due to local and distant earthquakes. J. Geophys. Res. 103, 869–889. https://doi.org/10.1029/97JB02335.
Rossi, G., Pastorutti, A., Nagy, I., Braitenberg, C., Parolai, S., 2021. Recurrence of fault valve behavior in a continental collision area: evidence from tilt/strain measurements in Northern Adria. Front. Earth Sci. 9, 641416. https://doi.org/10.3389/feart.2021.641416.
Rudnicki, J.W., 1999. Alteration of regional stress by reservoirs and other inhomogeneities: stabilizing or destabilizing?. In: Proceedings of the 9th International Congress on Rock Mechanics 3, pp. 1629–1637. ISRM-9CONGRESS-1999-303.
Ruiz-Barajas, S., Santoyo, M.A., Benito Oterino, M.B., Alvarado, G.E., Climent, A., 2019. Stress transfer patterns and local seismicity related to reservoir water-level variations. A case study in Central Costa Rica. Sci. Rep. 9, 5600. https://doi.org/10.1038/s41598-019-41890-y.
Rutqvist, J., Wu, Y.-S., Tsang, C.-F., Bodvarsson, G., 2002. A modeling approach for analysis of coupled multiphase fluid flow, heat transfer, and deformation in fractured porous rock. Int. J. Rock Mech. Min. Sci. 39, 429–442. https://doi.org/10.1016/S1365-1609(02)00022-9.
Rutqvist, J., Rinaldi, A.P., Cappa, F., Jeanne, P., Mazzoldi, A., Urpi, L., Guglielmi, Y., Vilarrasa, V., 2016. Fault activation and induced seismicity in geological carbon storage – Lessons learned from recent modeling studies. J. Rock Mech. Geotech. Eng. 8, 789–804. https://doi.org/10.1016/j.jrmge.2016.09.001.
Saffer, D.M., Tobin, H.J., 2011. Hydrogeology and mechanics of subduction zone forearcs: fluid flow and pore pressure. Annu. Rev. Earth Planet. Sci. 39, 157–186. https://doi.org/10.1146/annurev-earth-040610-133408.
Schoell, M., 1988. Multiple origins of methane in the Earth. Chem. Geol. 71, 1–10. https://doi.org/10.1016/0009-2541(88)90101-5.
Schoenball, M., Ajo-Franklin, J.B., Blankenship, D., Chai, C., Chakravarty, A., Dobson, P., Hopp, C., Kneafsey, T., Knox, H.A., Maceira, M., Robertson, M.C., Sprinkle, P., Strickland, C., Templeton, D., Schwering, P.C., Ulrich, C., Wood, T., The EGS Collab Team, 2020. Creation of a mixed-mode fracture network at mesoscale through hydraulic fracturing and shear stimulation. JGR Solid Earth 125, e2020JB019807. https://doi.org/10.1029/2020JB019807.
Scholz, C.H., 1998. Earthquakes and friction laws. Nature 391, 37–42. https://doi.org/10.1038/34097.
Scholz, C.H., 2002. The Mechanics of Earthquakes and Faulting, 2nd ed. Cambridge University Press. https://doi.org/10.1017/CBO9780511818516.
Scibek, J., 2020. Multidisciplinary database of permeability of fault zones and surrounding protolith rocks at world-wide sites. https://doi.org/10.6084/M9.FIGSHARE.10052033.V2.
Segall, P., 1989. Earthquakes triggered by fluid extraction. Geology 17, 942. https://doi.org/10.1130/0091-7613(1989)017<0942:ETBFE>2.3.CO;2.
Segall, P., 1992. Induced stresses due to fluid extraction from axisymmetric reservoirs. PAGEOPH 139, 535–560. https://doi.org/10.1007/BF00879950.
Segall, P., 2010. Earthquake and Volcano Deformation. Princeton University Press, Princeton, N.J.
Segall, P., Fitzgerald, S.D., 1998. A note on induced stress changes in hydrocarbon and geothermal reservoirs. Tectonophysics 289, 117–128. https://doi.org/10.1016/S0040-1951(97)00311-9.
Segall, P., Lu, S., 2015. Injection-induced seismicity: Poroelastic and earthquake nucleation effects. JGR Solid Earth 120, 5082–5103. https://doi.org/10.1002/2015JB012060.
Segall, P., Rice, J.R., 1995. Dilatancy, compaction, and slip instability of a fluid-infiltrated fault. J. Geophys. Res. 100, 22155–22171. https://doi.org/10.1029/95JB02403.
Segall, P., Jónsson, S., Ágústsson, K., 2003. When is the strain in the meter the same as the strain in the rock? Geophys. Res. Lett. 30, 2003GL017995. https://doi.org/10.1029/2003GL017995.
Sellin, P., Leupin, O.X., 2013. The use of clay as an engineered barrier in radioactive-waste management — a review. Clay Clay Miner. 61, 477–498. https://doi.org/10.1346/CCMN.2013.0610601.
Selvadurai, A.P.S., Suvorov, A.P., 2016. Thermo-Poroelasticity and Geomechanics, 1st ed. Cambridge University Press. https://doi.org/10.1017/CBO9781316543832.
Shapiro, S.A., 2015. Fluid-Induced Seismicity, 1st ed. Cambridge University Press. https://doi.org/10.1017/CBO9781139051132.
Shapiro, S.A., 2018. Seismogenic index of underground fluid injections and productions. JGR Solid Earth 123, 7983–7997. https://doi.org/10.1029/2018JB015850.
Shapiro, S.A., Dinske, C., Langenbruch, C., Wenzel, F., 2010. Seismogenic index and magnitude probability of earthquakes induced during reservoir fluid stimulations. Lead. Edge 29, 304–309. https://doi.org/10.1190/1.3353727.
Sibson, R.H., 1973. Interactions between temperature and pore-fluid pressure during earthquake faulting and a mechanism for partial or total stress relief. Nat. Phys. Sci. 243, 66–68. https://doi.org/10.1038/physci243066a0.
Sibson, R.H., 1990. Conditions for fault-valve behaviour. SP 54, pp. 15–28. https://doi.org/10.1144/GSL.SP.1990.054.01.02.
Sigurdsson, H., 2000. Encyclopedia of Volcanoes. Academic Press, San Diego.
Silverii, F., Maccaferri, F., Richter, G., Gonzalez Cansado, B., Wang, R., Hainzl, S., Dahm, T., 2021. Poroelastic model in a vertically sealed gas storage: a case study from cyclic injection/production in a carbonate aquifer. Geophys. J. Int. 227, 1322–1338. https://doi.org/10.1093/gji/ggab268.
Sirorattanakul, K., Ross, Z.E., Khoshmanesh, M., Cochran, E.S., Acosta, M., Avouac, J., 2022. The 2020 Westmorland, California Earthquake Swarm as aftershocks of a slow slip event sustained by fluid flow. JGR Solid Earth 127, e2022JB024693. https://doi.org/10.1029/2022JB024693.
Skempton, A.W., 1954. The pore-pressure coefficients *A* and *B*. Géotechnique 4, 143–147. https://doi.org/10.1680/geot.1954.4.4.143.
Smith, J.D., Heimisson, E.R., Bourne, S.J., Avouac, J.-P., 2022. Stress-based forecasting of induced seismicity with instantaneous earthquake failure functions: applications to the Groningen gas reservoir. Earth Planet. Sci. Lett. 594, 117697. https://doi.org/10.1016/j.epsl.2022.117697.
Steacy, S., Gomberg, J., Cocco, M., 2005. Introduction to special section: stress transfer, earthquake triggering, and time-dependent seismic hazard. J. Geophys. Res. 110, 2005JB003692. https://doi.org/10.1029/2005JB003692.
Stissi, S.C., Currenti, G., Cannavò, F., Napoli, R., 2023. Evidence of poro-elastic inflation at the onset of the 2021 Vulcano Island (Italy) unrest. Front. Earth Sci. 11, 1179095. https://doi.org/10.3389/feart.2023.1179095.
Subedi, M., Acharya, I.P., 2022. Liquefaction hazard assessment and ground failure probability analysis in the Kathmandu Valley of Nepal. Geoenviron. Disasters 9, 1. https://doi.org/10.1186/s40677-021-00203-0.
Tao, J., Wu, Y., Elsworth, D., Li, P., Hao, Y., 2019. Coupled thermo-hydro-mechanical-chemical modeling of permeability evolution in a CO $_2$ -circulated geothermal reservoir. Geofluids 2019, 1–15. https://doi.org/10.1155/2019/5210730.
Teatini, P., Ferronato, M., Gambolati, G., Gonella, M., 2006. Groundwater pumping and land subsidence in the Emilia-Romagna coastland, Italy: Modeling the past occurrence and the future trend. Water Resour. Res. 42, 2005WR004242. https://doi.org/10.1029/2005WR004242.
Terzaghi, K., 1943. Theoretical Soil Mechanics, 1st ed. Wiley. https://doi.org/10.1002/9780470172766.
Todesco, M., 2021. Caldera's breathing: poroelastic ground deformation at Campi Flegrei (Italy). Front. Earth Sci. 9, 702665. https://doi.org/10.3389/feart.2021.702665.
Todesco, M., Berrino, G., 2005. Modeling hydrothermal fluid circulation and gravity signals at the Phlegraean Fields caldera. Earth Planet. Sci. Lett. 240, 328–338. https://doi.org/10.1016/j.epsl.2005.09.016.

Todesco, M., Chiodini, G., Macedonio, G., 2003. Monitoring and modelling hydrothermal fluid emission at La Solfatara (Phlegrean Fields, Italy). An interdisciplinary approach to the study of diffuse degassing. J. Volcanol. Geotherm. Res. 125, 57–79. https://doi.org/10.1016/S0377-0273(03)00089-1.

Todesco, M., Rinaldi, A.P., Bonafede, M., 2010. Modeling of unrest signals in heterogeneous hydrothermal systems. J. Geophys. Res. 115, 2010JB007474. https://doi.org/10.1029/2010JB007474.

Todesco, M., Rouwet, D., Nespoli, M., Bonafede, M., 2015. How steep is my seep? Seepage in volcanic lakes, hints from numerical simulations. In: Rouwet, D., Christenson, B., Tassi, F., Vandemeulebrouck, J. (Eds.), Volcanic Lakes. Springer Berlin Heidelberg, Berlin, Heidelberg, pp. 323–339. https://doi.org/10.1007/978-3-642-36833-2_14.

Tramelli, A., Godano, C., Ricciolino, P., Giudicepietro, F., Caliro, S., Orazi, M., De Martino, P., Chiodini, G., 2021. Statistics of seismicity to investigate the Campi Flegrei caldera unrest. Sci. Rep. 11, 7211. https://doi.org/10.1038/s41598-021-86506-6.

Trasatti, E., Bonafede, M., Ferrari, C., Giunchi, C., Berrino, G., 2011. On deformation sources in volcanic areas: Modeling the Campi Flegrei (Italy) 1982–84 unrest. Earth Planet. Sci. Lett. 306, 175–185. https://doi.org/10.1016/j.epsl.2011.03.033.

Trutnevyte, E., Wiemer, S., 2017. Tailor-made risk governance for induced seismicity of geothermal energy projects: an application to Switzerland. Geothermics 65, 295–312. https://doi.org/10.1016/j.geothermics.2016.10.006.

Tsang, C.F., Barnichon, J.D., Birkholzer, J., Li, X.L., Liu, H.H., Sillen, X., 2012. Coupled thermo-hydro-mechanical processes in the near field of a high-level radioactive waste repository in clay formations. Int. J. Rock Mech. Min. Sci. 49, 31–44. https://doi.org/10.1016/j.ijrmms.2011.09.015.

Turcotte, D., Schubert, G., 2014. Geodynamics, 3rd ed. Cambridge University Press. https://doi.org/10.1017/CBO9780511843877.

Urpi, L., Rinaldi, A.P., Rutqvist, J., Wiemer, S., 2019. Fault stability perturbation by thermal pressurization and stress transfer around a deep geological repository in a clay formation. JGR Solid Earth 124, 8506–8518. https://doi.org/10.1029/2019JB017694.

Van Der Elst, N.J., Page, M.T., Weiser, D.A., Goebel, T.H.W., Hosseini, S.M., 2016. Induced earthquake magnitudes are as large as (statistically) expected. JGR Solid Earth 121, 4575–4590. https://doi.org/10.1002/2016JB012818.

Van Duijn, C.J., Mikelić, A., 2023. Mathematical theory of nonlinear single-phase poroelasticity. J. Nonlinear Sci. 33, 44. https://doi.org/10.1007/s00332-023-09896-z.

Van Thienen-Visser, K., Breunese, J.N., 2015. Induced seismicity of the Groningen gas field: history and recent developments. Lead. Edge 34, 664–671. https://doi.org/10.1190/tle34060664.1.

Vasilyeva, M., Tyrylgin, A., 2021. Machine learning for accelerating macroscopic parameters prediction for poroelasticity problem in stochastic media. Comput. Math. Appl. 84, 185–202. https://doi.org/10.1016/j.camwa.2020.09.024.

Verdon, J.P., Stork, A.L., Bissell, R.C., Bond, C.E., Werner, M.J., 2015. Simulation of seismic events induced by CO2 injection at in Salah, Algeria. Earth Planet. Sci. Lett. 426, 118–129. https://doi.org/10.1016/j.epsl.2015.06.029.

Vilarrasa, V., Rutqvist, J., Rinaldi, A.P., 2015. Thermal and capillary effects on the caprock mechanical stability at in Salah, Algeria. Greenh. Gases 5, 449–461. https://doi.org/10.1002/ghg.1486.

Vilarrasa, V., Rinaldi, A.P., Rutqvist, J., 2017. Long-term thermal effects on injectivity evolution during CO2 storage. Int. J. Greenh. Gas Contr. 64, 314–322. https://doi.org/10.1016/j.ijggc.2017.07.019.

Vilarrasa, V., Carrera, J., Olivella, S., Rutqvist, J., Laloui, L., 2019. Induced seismicity in geologic carbon storage. Solid Earth 10, 871–892. https://doi.org/10.5194/se-10-871-2019.

Viswanathan, H.S., Ajo-Franklin, J., Birkholzer, J.T., Carey, J.W., Guglielmi, Y., Hyman, J.D., Karra, S., Pyrak-Nolte, L.J., Rajaram, H., Srinivasan, G., Tartakovsky, D.M., 2022. From fluid flow to coupled processes in fractured rock: recent advances and new frontiers. Rev. Geophys. 60, e2021RG000744. https://doi.org/10.1029/2021RG000744.

Voss, C.I., Provost, A.M., 2002. SUTRA: A Model for 2D or 3D Saturated-Unsaturated, Variable-Density Ground-Water Flow with Solute or Energy Transport. https://doi.org/10.3133/wri024231.

Walter, M.J., 2021. Water transport to the core–mantle boundary. Natl. Sci. Rev. 8, nwab007. https://doi.org/10.1093/nsr/nwab007.

Wang, H.F., 2000. Theory of Linear Poroelasticity with Applications to Geomechanics and Hydrogeology. Princeton University Press.

Wang, C., Chia, Y., 2008. Mechanism of water level changes during earthquakes: near field versus intermediate field. Geophys. Res. Lett. 35, 2008GL034227. https://doi.org/10.1029/2008GL034227.

Wang, R., Kümpel, H., 2003. Poroelasticity: Efficient modeling of strongly coupled, slow deformation processes in a multilayered half-space. Geophysics 68, 705–717. https://doi.org/10.1190/1.1567241.

Wang, C., Manga, M., 2010. Hydrologic responses to earthquakes and a general metric. Geofluids 10, 206–216. https://doi.org/10.1111/j.1468-8123.2009.00270.x.

Wang, C., Manga, M., 2014. Earthquakes and water. In: Meyers, R.A. (Ed.), Encyclopedia of Complexity and Systems Science. Springer New York, New York, NY, pp. 1–38. https://doi.org/10.1007/978-3-642-27737-5_606-1.

Wang, C.-Y., Manga, M., 2021a. Water and Earthquakes. In: Lecture Notes in Earth System Sciences. Springer International Publishing, Cham. https://doi.org/10.1007/978-3-030-64308-9.

Wang, C.-Y., Manga, M., 2021b. Groundwater level. In: Water and Earthquakes. Springer International Publishing, Cham, pp. 155–200. https://doi.org/10.1007/978-3-030-64308-9_6.

Wang, C., Cheng, L.-H., Chin, C.-V., Yu, S.-B., 2001. Coseismic hydrologic response of an alluvial fan to the 1999 Chi-Chi earthquake, Taiwan. Geology 29, 831. https://doi.org/10.1130/0091-7613(2001)029<0831:CHROAA>2.0.CO;2.

Wang, B., Liu, Y., Sun, X., Ma, Y., Zhang, L., Ren, H., Fang, Z., 2018. Hydrogeological and geochemical observations for earthquake prediction research in china: a brief overview. Pure Appl. Geophys. 175, 2541–2555. https://doi.org/10.1007/s00024-018-1885-y.

White, M.D., Oostrom, M., 2006. STOMP Subsurface Transport Over Multiple Phases. User Guide: Subsurface Transport Over Multiple Phases. June 2006 Contract: DE-AC05-76RL01830. Available online. https://www.pnnl.gov/main/publications/external/technical_reports/PNNL-15782.pdf.

Wibberley, C.A.J., 2014. Hydraulic diffusivity of fault gouge zones and implications for thermal pressurization during seismic slip. Earth Planet Sp. 54, 1153–1171. https://doi.org/10.1186/BF03353317.

Woodman, N.D., Burgess, W.G., Ahmed, K.M., Zahid, A., 2019. A partially coupled hydro-mechanical analysis of the Bengal Aquifer System under hydrological loading. Hydrol. Earth Syst. Sci. 23, 2461–2479. https://doi.org/10.5194/hess-23-2461-2019.

Xie, L., Min, K.-B., Song, Y., 2015. Observations of hydraulic stimulations in seven enhanced geothermal system projects. Renew. Energy 79, 56–65. https://doi.org/10.1016/j.renene.2014.07.044.

Xu, T., Sonnenthal, E., Spycher, N., Pruess, K., 2008. TOUGHREACT User's Guide: A simulation program for Nonisothermal Multiphase Reactive Geochemical Transport in Variably Saturated Geologic Media. V1.2.1-LBNL-55460-2008, vol. 32. Lawrence Berkeley National Lab. (LBNL), Berkeley, CA, USA, pp. 1–206.

Yang, X., Davis, P.M., Dieterich, J.H., 1988. Deformation from inflation of a dipping finite prolate spheroid in an elastic half-space as a model for volcanic stressing. J. Geophys. Res. 93, 4249–4257. https://doi.org/10.1029/JB093iB05p04249.

Yang, Haozhe, Guo, R., Zhou, J., Yang, Hongfeng, Sun, H., 2022. Transient poroelastic response to megathrust earthquakes: a look at the 2015 *M* w 8.3 Illapel, Chile, event. Geophys. J. Int. 230, 908–915. https://doi.org/10.1093/gji/ggac099.

Yu, H., Harrington, R.M., Liu, Y., Wang, B., 2019. Induced seismicity driven by fluid diffusion revealed by a near-field hydraulic stimulation monitoring array in the Montney Basin, British Columbia. JGR Solid Earth 124, 4694–4709. https://doi.org/10.1029/2018JB017039.

Yu, H., Liu, L., Ma, Yuchuan, Yan, R., Liu, J., Ma, Yawei, Li, Z., Zhang, X., Zhao, J., Yu, C., 2023. Observed hydrological changes associated with active tectonic blocks before three consecutive earthquakes in Qinghai, China. Sci. Rep. 13, 8988. https://doi.org/10.1038/s41598-023-36274-2.

Yuono, R.T., Daud, Y., 2020. Reservoir simulation of Ulumbu geothermal field using TOUGH2 and ITOUGH2 simulator. IOP Conf. Ser. Earth Environ. Sci. 538, 012059. https://doi.org/10.1088/1755-1315/538/1/012059.

Zang, A., Oye, V., Jousset, P., Deichmann, N., Gritto, R., McGarr, A., Majer, E., Bruhn, D., 2014. Analysis of induced seismicity in geothermal reservoirs – an overview. Geothermics 52, 6–21. https://doi.org/10.1016/j.geothermics.2014.06.005.

Zappone, A., Rinaldi, A.P., Grab, M., Wenning, Q.C., Roques, C., Madonna, C., Obermann, A.C., Bernasconi, S.M., Brennwald, M.S., Kipfer, R., Soom, F., Cook, P., Guglielmi, Y., Nussbaum, C., Giardini, D., Mazzotti, M., Wiemer, S., 2021. Fault sealing and caprock integrity for CO_2 storage: an in situ injection experiment. Solid Earth 12, 319–343. https://doi.org/10.5194/se-12-319-2021.

Zbinden, D., Rinaldi, A.P., Urpi, L., Wiemer, S., 2017. On the physics-based processes behind production-induced seismicity in natural gas fields. JGR Solid Earth 122, 3792–3812. https://doi.org/10.1002/2017JB014003.

Zbinden, D., Rinaldi, A.P., Diehl, T., Wiemer, S., 2020a. Potential influence of overpressurized gas on the induced seismicity in the St. Gallen deep geothermal project (Switzerland). Solid Earth 11, 909–933. https://doi.org/10.5194/se-11-909-2020.

Zbinden, D., Rinaldi, A.P., Diehl, T., Wiemer, S., 2020b. Hydromechanical modeling of fault reactivation in the St. Gallen Deep Geothermal Project (Switzerland): poroelasticity or hydraulic connection? Geophys. Res. Lett. 47, e2019GL085201. https://doi.org/10.1029/2019GL085201.

Zencher, F., Bonafede, M., Stefansson, R., 2006. Near-lithostatic pore pressure at seismogenic depths: a thermoporoelastic model. Geophys. J. Int. 166, 1318–1334. https://doi.org/10.1111/j.1365-246X.2006.03069.x.

Zeng, Z., Grigg, R., 2006. A criterion for non-darcy flow in porous media. Transp. Porous Media 63, 57–69. https://doi.org/10.1007/s11242-005-2720-3.

Zeng, Y.-C., Su, Z., Wu, N.-Y., 2013. Numerical simulation of heat production potential from hot dry rock by water circulating through two horizontal wells at Desert Peak geothermal field. Energy 56, 92–107. https://doi.org/10.1016/j.energy.2013.04.055.

Zhang, L., Bai, T., Zhao, Q., Zhang, X., Cheng, H., Li, Z., 2023. CO2 injection for enhanced gas recovery and geo-storage in complex tight sandstone gas reservoirs. Processes 11, 2059. https://doi.org/10.3390/pr11072059.

Zhao, D., Kitagawa, H., Toyokuni, G., 2015. A water wall in the Tohoku forearc causing large crustal earthquakes. Geophys. J. Int. 200, 149–172. https://doi.org/10.1093/gji/ggu381.

Zhu, W., Allison, K.L., Dunham, E.M., Yang, Y., 2020. Fault valving and pore pressure evolution in simulations of earthquake sequences and aseismic slip. Nat. Commun. 11, 4833. https://doi.org/10.1038/s41467-020-18598-z.

Zimmermann, G., Reinicke, A., 2010. Hydraulic stimulation of a deep sandstone reservoir to develop an Enhanced Geothermal System: Laboratory and field experiments. Geothermics 39, 70–77. https://doi.org/10.1016/j.geothermics.2009.12.003.